CHEMISTRY
AN ASIAN JOURNAL

DOI: 10.1002/asia.200700082

One-Dimensional, Cofacial Porphyrin Polymers Formed by Self-Assembly of *meso*-Tetrakis(ERE Donor) Zinc(II) Porphyrins

Bart M. J. M. Suijkerbuijk,[a] Duncan M. Tooke,[b] Anthony L. Spek,[b] Gerard van Koten,[a] and Robertus J. M. Klein Gebbink*[a]

Abstract: A series of *meso*-tetrakis-(ERE donor) zinc(II) porphyrins ***n*Zn** (ERE donor = 4-R-3,5-bis[(E)-methyl]-phenyl; **1**Zn: E = NMe_2, R = Br; **2**Zn: E = NMe_2, R = H; **3**Zn: E = OMe, R = Br; **4**Zn: E = OMe, R = H) have been synthesized in excellent yields. As a result of the combination of a Lewis acidic site and eight Lewis basic sites within one molecule, monomeric molecules of ***n*Zn** self-assemble to form one-dimensional porphyrin polymers $[\boldsymbol{n}Zn]_\infty$ in the solid state, as confirmed for **1**Zn and **3**Zn by X-ray crystallography. The coordination environment around the zinc(II) ions in these polymers is octahedral. They are ligated by four equatorial nitrogen atoms of the porphyrin and two apical E atoms (E = N, O) provided by the EBrE donor groups of adjacent ***n*Zn** molecules. Complexes **2**Zn and **4**Zn did not form single crystals, but solid-state UV/Vis analysis points to the formation of similar structures. Solution UV/Vis and ^{1}H NMR spectroscopy indicated that interactions between **1**Zn and **2**Zn monomers in the polymers are stronger than between **3**Zn and **4**Zn monomers. Interestingly, they also revealed that the presence of a neighboring bromine atom in the EBrE donor groups has a considerable influence on the coordination properties of the benzylic N or O atoms. The zinc(II) ions of the porphyrins most likely adopt only hexacoordination in the solid state, owing to the unique predisposition of Lewis acidic and basic sites in the ***n*Zn** molecules. Several parameters of the aggregates, for example, the interplanar separation between porphyrins and the zinc–zinc distances, change as a function of the coordinating E groups. The high degree of modularity in their synthesis makes these zinc(II) porphyrins an interesting new entry in noncovalent multiporphyrin assemblies.

Keywords: chlorophylls · coordination modes · porphyrins · self-assembly · zinc

Introduction

One-, two-, and three-dimensional porphyrin arrays continue to attract attention because of their relevance to biological systems such as the light-harvesting apparatus in plants, algae, and bacteria.[1–8] Numerous reports have dealt with the design, synthesis, and applications of covalently linked multiporphyrin arrays.[9–14] Nature uses noncovalent interactions to assemble these chromophores; therefore, an increasing amount of research is focused on the synthesis of multiporphyrin arrays through self-assembly. The self-assembly of these arrays relies on coordination[15–24] and/or hydrogen bonds,[25] and the formed structures can thus be highly dynamic. One-dimensional polymeric multiporphyrin assemblies, in which the metal in the porphyrin center is used as a connector, are being investigated in particular. These structures can be created by combining A–A- and B–B-type monomers, which can form alternating copolymers of the form $[\cdot\cdot A–A\cdots B–B\cdot\cdot]_\infty$. The monomers generally consist of a metalloporphyrin capable of accommodating two axial ligands (on either face of the porphyrin plane) and an α,ω-ditopic ligand. Several combinations have been investigated, including those of ruthenium(II) porphyrins with diphosphine ligands,[26] phosphorus(V) porphyrins with oxygen ligands,[27,28] and manganese(III) porphyrins with 4,4′-bipyridyl ligands.[29] Polymers formed from polycyanoalkenes and

[a] Dr. B. M. J. M. Suijkerbuijk, Prof. Dr. G. van Koten, Prof. Dr. R. J. M. Klein Gebbink
Organic Chemistry and Catalysis
Faculty of Science, Utrecht University
Padualaan 8, 3584 CH, Utrecht (The Netherlands)
Fax: (+31) 30-252-3615
E-mail: r.j.m.kleingebbink@chem.uu.nl

[b] Dr. D. M. Tooke, Prof. Dr. A. L. Spek
Crystal and Structural Chemistry
Faculty of Science, Utrecht University
Padualaan 8, 3584 CH, Utrecht (The Netherlands)

Supporting information for this article is available on the WWW under http://www.chemasianj.org or from the author.

manganese(II)[30–32] or iron(III) porphyrins[33] were prepared by Miller and co-workers. Porphyrin coordination polymers consisting of A–B-type monomers (thus forming $[\cdot\cdot A–B\cdot\cdot]_\infty$ polymers or cyclic oligomers) have also been studied thoroughly. For this type of polymers, metalloporphyrins with covalently attached Lewis bases were used as the monomeric parts. To prevent intramolecular coordination, both the length and the conformational rigidity of the linker between the Lewis basic moiety and the Lewis acidic metalloporphyrin part play important roles. At the same time, these parameters can also be used to optimize intermolecular interactions, thus leading to polymer or ring formation. The connectivity between the monomers may be single or twofold, depending on the flexibility of the A–B linkage and on whether the metal in the porphyrin can accommodate one (Zn,[34–40] $Co(O_2)$[41]) or two axial ligands (Cu^{II},[42] Co^{II},[43] Co^{III}[44]).

We started a research project about the design and synthesis of multitopic ligand systems, particularly tetrakis(ECE pincer–metal) metalloporphyrin hybrids (Scheme 1, top).[45] These hybrids consist of a (metallo)porphyrin core surrounded by four ECE-pincer–metal groups (with ECE pincer being the monoanionic, potentially tridentate ligand $[2,6\text{-}(ECH_2)_2C_6H_3]^-$ (E = NR_2, OR, PR_2, SR)),[46] which are connected via their *para* positions to the respective *meso* positions on the porphyrin. After synthesizing the tetrakis(ECE pincer–metal) free-base porphyrin hybrids (Scheme 1, top; M^1 = 2H), we targeted the corresponding heteromultimetallic systems (Scheme 1, top; M^1 = metal) as our next synthetic objectives. In this context, the question arose as to whether the pincer metal would be put in place after metalation of the porphyrin or vice versa. With regard to the former approach, the introduction of a metal into the central porphyrin cavity could give rise to the formation of

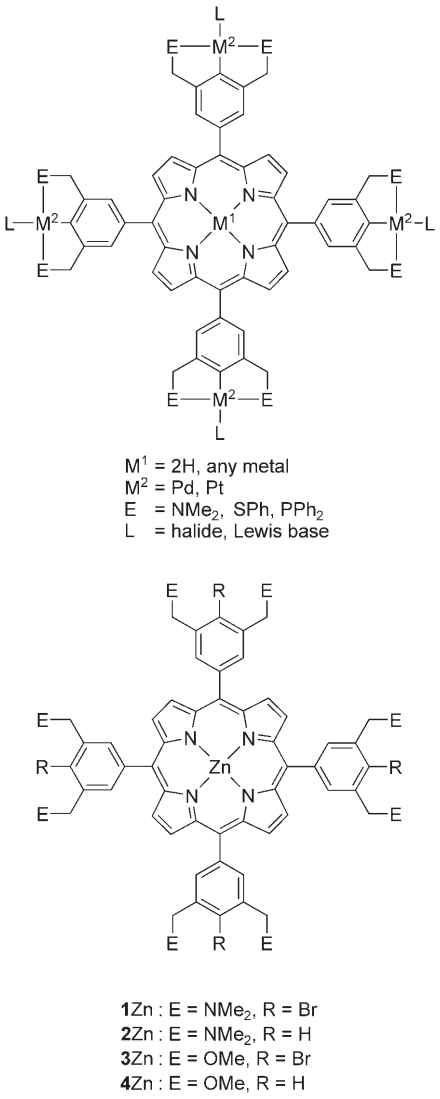

Scheme 1. General formulae of the multimetallic pincer-porphyrin hybrids (top) and the tetrakis(ERE donor) zinc(II) porphyrins (bottom) described herein.

Abstract in Dutch: Een viertal zinkporfyrines ***n*Zn** met elk vier *meso*-ERE-donorgroepen (ERE donor = 4-R-3,5-bis[(E)-methyl]fenyl; **1**Zn: NBrN-groepen; **2**Zn: NHN-groepen; **3**Zn: OBrO-groepen; **4**Zn: OHO-groepen) is in uitstekende opbrengsten gesynthetiseerd. Doordat zij bestaan uit een unieke combinatie van Lewis-zure en Lewis-basische groepen, zelf-assembleren deze moleculen tot ééndimensionale, supramoleculaire coördinatiepolymeren met de algemene formule $[\boldsymbol{n}Zn]_\infty$, hetgeen werd bewezen door éénkristal Röntgenkristallografie aan **1**Zn en **3**Zn. De zink(II) ionen in deze polymeren zijn octaëdrisch omringd door zes liganden; vier equatoriale ligandposities worden ingenomen door de pyrroolstikstofatomen van de porfyrine, terwijl de twee apicale posities bezet worden door de O of N atomen van de donorgroepen. Zinkporfyrines **2**Zn en **4**Zn vormen geen éénkristallen, maar vaste stof UV/Vis metingen wezen op de vorming van soortgelijke structuren. UV/Vis en ^{1}H NMR data wijzen er verder op dat de interacties tussen de **1**Zn en **2**Zn monomeren veel sterker zijn dan de interacties tussen **3**Zn en **4**Zn monomeren. Ook duiden zij op een grote invloed van broomatomen in de nabijheid van de donorgroepen in **1**Zn en **3**Zn op de coördinatie-eigenschappen. Verder is gevonden dat de speciale hexacoördinatie alleen optreedt in de vaste stof en niet zozeer in oplossing. Eén van de redenen voor de vorming van deze interessante polymeren is de overmaat aan Lewis-basische groepen en hun relatieve, ruimtelijke oriëntatie ten opzichte van de zinkcentra. De gevormde structuren lijken sterk op de in de natuur aanwezige bacteriochlorofyllaggregaten die lichtenergie van de zon omzetten in chemische energie. Zoals uit de kristallografische analyse blijkt, hangen enkele belangrijke structurele parameters van de polymeren af van het Lewis basische donor atoom. Omdat de ***n*Zn** verbindingen eenvoudig te modificeren zijn, vormen zij een interessante aanvulling op eerdere niet-covalent gebonden porfyrinepolymeren.

higher-order aggregates between these molecules, as the resulting tetrakis(ERE donor) metalloporphyrins (ERE donor = 4-R-3,5-bis[(E)-methyl]phenyl; E = NMe_2, OMe, SPh, PPh_2; R = H, Br) comprise eight Lewis basic and one or more Lewis acidic sites (depending on the metal); that is, aggregates of type $[\cdot\cdot A–B\cdot\cdot]_\infty$ may be envisioned for these systems. We therefore decided to investigate the supramolecular chemistry of several tetrakis(ERE donor) zinc(II) porphyrins (Scheme 1, bottom) that bear either nitrogen (**1**Zn and **2**Zn**)** or oxygen (**3**Zn and **4**Zn) Lewis basic sites.

Herein we report the synthesis and the solid-state and solution structures of the zinc(II) porphyrins **1**Zn–**4**Zn. To understand the coordination chemistry of these systems in more detail, we also analyzed the assembly behavior of a series of mono- and bidentate Lewis bases with [*meso*-tetraphenylporphyrinato]zinc(II) (ZnTPP).

Results

Synthesis

Multitopic ligands **1**–**4**[45,47] were treated with $Zn(OAc)_2{\cdot}2H_2O$ in a mixture of CH_2Cl_2 and MeOH to yield the corresponding zinc(II) complexes **1**Zn–**4**Zn in essentially quantitative yields (Scheme 2). During each metalation reaction, a common color change of the reaction mixture was observed from dark red (free-base compounds **1**–**4**) to light pink (**1**Zn–**4**Zn). UV/Vis spectroscopic monitoring of the reaction progress showed a change from the four-Q-band spectrum of the free-base porphyrin to the two-Q-band spectrum of its zinc(II) complex. Purification of these compounds was performed by layering solutions of CH_2Cl_2 with hexane. In this way, **1**Zn and **3**Zn were isolated as red crystalline solids and **2**Zn and **4**Zn were obtained as purple solids in essentially quantitative yields.

As it was reported that *N,N*-dimethylbenzylamine groups readily react with $^1O_2$,[48] and given the ability of zinc(II) porphyrins to act as photosensitizers, caution was taken to avoid contact of **1**, **2**, **1**Zn, and **2**Zn with air and light. The identity and sample homogeneity of all compounds were confirmed by ^1H and $^{13}C\{^1H\}$ NMR spectroscopy, mass spectrometry, UV/Vis spectroscopy, and elemental analysis (see Experimental Section).

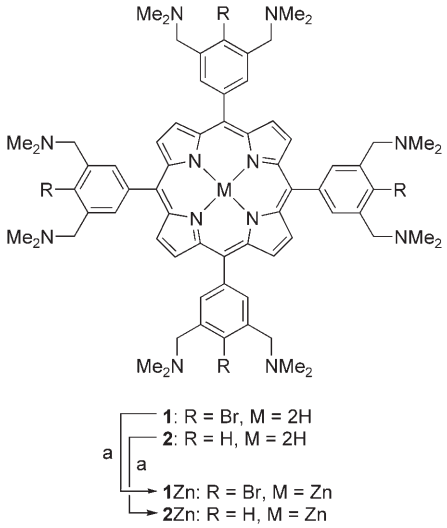

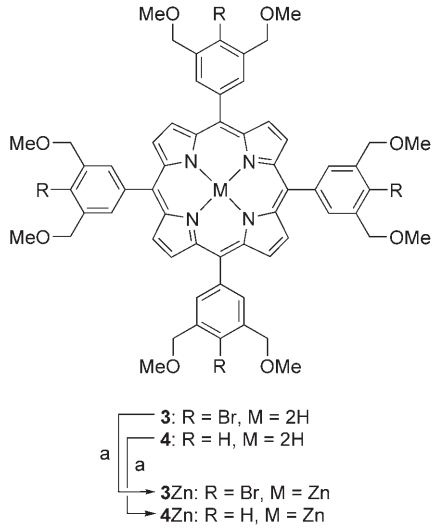

Scheme 2. Synthesis of **1**Zn–**4**Zn. a) $Zn(OAc)_2{\cdot}2H_2O$, $MeOH/CH_2Cl_2$.

Crystallography

Single crystals of **1**Zn and **3**Zn of X-ray quality were obtained by layering solutions of these compounds in dichloromethane with hexane. Their molecular structures in the solid state are depicted in Figure 1, and the crystallographic details are shown in Table 1. Both structures feature a zinc(II) porphyrin core, which is tetrasubstituted at its four *meso*-positions with 3,5-bis[(dimethylamino)methyl]-4-bromophenyl and 3,5-bis(methoxymethyl)-4-bromophenyl groups, respectively. In each structure, the zinc atom is located at the center of the porphyrin ring with $Zn–N_{pyrrole}$ bond lengths of 2.050(4)–2.054(4) Å. Both structures are centrosymmetric with the zinc atom as the inversion point. The porphyrin parts of both **1**Zn and **3**Zn adopt *wav*-type nonplanar deformation modes.[49] Two of the *meso*-phenyl groups, which are positioned in a *trans* manner with respect to the porphyrin core, have a normal position. The other two *meso*-phenyl groups are bent quite markedly with respect to the porphyrin plane; the Zn–C1–C2 (**1**Zn) and Zn–C3–C4 (**3**Zn) angles are 170.3(4) and 166.22(19)°, respectively. The torsion angles between the porphyrin planes and the phenyl groups are 75.9(8) and 57.4(4)° for **1**Zn, and 75.8(2) and 65.8(3)° for **3**Zn.

The crystal structures one level of organization higher reveal that both compounds self-assemble into one-dimensional coordination polymers of general formula $[\boldsymbol{n}Zn]_\infty$ with highly similar structures, as shown for $[\mathbf{1}Zn]_\infty$ in Figure 2. In the solid state structure of $[\mathbf{1}Zn]_\infty$, the zinc atoms are surrounded in an octahedral manner,[50] with four equatorial pyrrolic nitrogen donor atoms provided by the

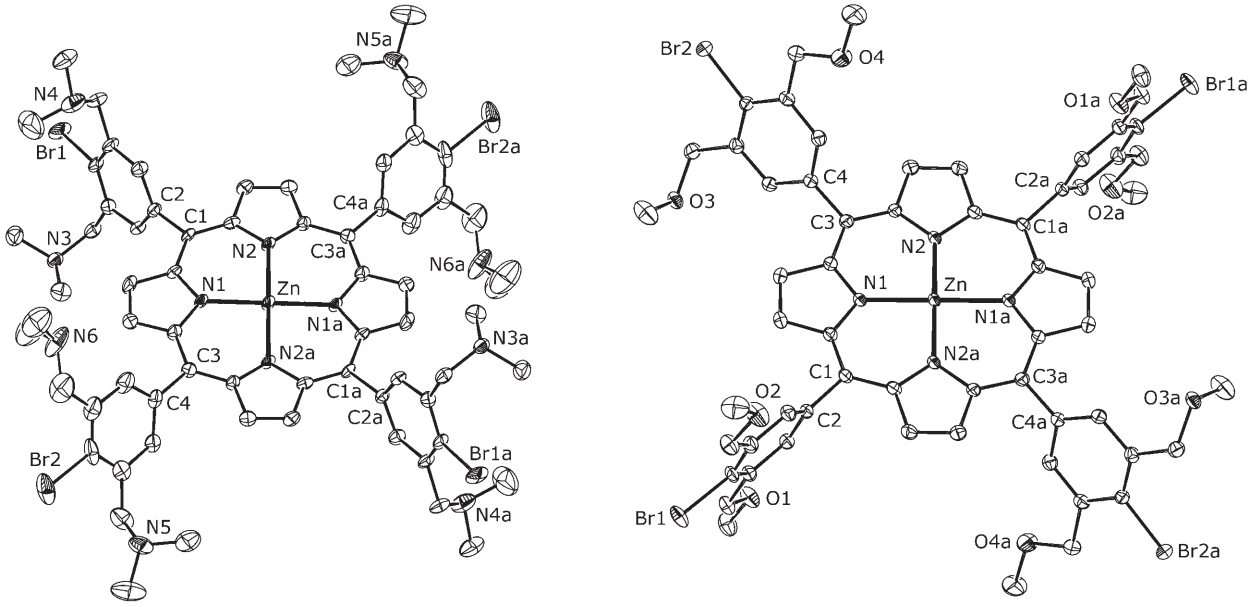

Figure 1. Molecular structures of **1**Zn (left) and **3**Zn (right) at 50% probability. Hydrogen atoms, solvent molecules, and disordered dimethylamino groups (**1**Zn) are omitted for clarity.

Table 1. Crystallographic information.

	1Zn	**3**Zn	NBrN–$(ZnTPP)_2$	DMBABr–ZnTPP	H_2O–ZnTPP	DMBA–ZnTPP
Formula	$C_{68}H_{80}Br_4N_{12}Zn$	$C_{60}H_{56}Br_4N_4O_8Zn\cdot 2(CH_2Cl_2)$	$C_{100}H_{75}BrN_{10}Zn_2$	$C_{53}H_{40}BrN_5Zn$	$C_{44}H_{30}N_4OZn$	$C_{53}H_{41}N_5Zn$
M_r	1450.43[a]	1515.95	1627.35	892.18	696.09	813.28
Space group	$P\bar{1}$ (No. 2)	$P\bar{1}$ (No. 2)	$P\bar{1}$ (No. 2)	$P\bar{1}$ (No. 2)	$I4/m$ (No. 87)	$P\bar{1}$ (No. 2)
a [Å]	9.932(2)	8.7503(8)	11.0729(4)	11.7041(6)	13.3504(10)	11.4716(9)
b [Å]	14.055(4)	12.9441(8)	12.9265(7)	12.0847(10)	13.3504(10)	11.9800(8)
c [Å]	14.946(3)	15.1577(10)	14.5903(6)	15.9026(9)	9.6034(10)	16.2244(10)
α [°]	113.188(15)	113.520(5)	74.824(4)	88.440(6)	90	87.676(6)
β [°]	103.561(18)	96.938(8)	72.176(3)	85.168(5)	90	83.657(4)
γ []	99.86(2)	97.479(7)	83.884(4)	68.161(5)	90	69.038(5)
V [Å^3]	1781.4(8)	1532.4(2)	1918.00(16)	2080.4(2)	1711.6(3)	2069.4(3)
d_x [g cm^{-3}]	1.352[a]	1.643	1.409	1.424	1.351	1.305
Z	1	1	1	2	2	2
μ ($Mo_{K\alpha}$) [mm^{-1}]	2.634[a]	3.241	1.205	1.595	0.759	0.637
Crystal size [mm]	0.09×0.12×0.33	0.06×0.07×0.43	0.15×0.20×0.20	0.15×0.15×0.30	0.07×0.19×0.21	0.19×0.25×0.32
Color	dark red	red	red	dark red	dark red	dark red
T [K]	150	150	150	150	150	150
θ_{min}, θ_{max} [°]	1.6, 23.0	1.5, 26.0	1.5, 27.5	1.8, 27.5	2.2, 27.4	1.8, 27.5
Total unique data	21534, 4956	28965, 6013	52932, 8748	57368, 9518	7948, 1050	59100, 9467
Observed ($I > 2\sigma(I)$)	3911	5396	7559	7625	855	7943
N_{ref}, N_{par}	4956, 423	6013, 380	8748, 504	9518, 543	1050, 72	9467, 534
R,[b] $wR2$[c]	0.0516, 0.1397	0.0363, 0.092	0.0404, 0.0980	0.0332, 0.0779	0.0387, 0.0951	0.0325, 0.0786
S	1.08	1.02	1.12	1.04	1.06	1.03
ρ_{min}, ρ_{max} [e Å^{-3}]	−1.08, 1.64	−1.50, 1.26	−0.63, 0.86	−0.78, 0.94	−0.34, 0.30	−0.32, 0.37

[a] Disordered solvent contribution not taken into account. [b] $R = \Sigma|F_0 - F_c|/\Sigma F_0$. [c] $wR2 = [\Sigma w(F_0^2 - F_c^2)^2/\Sigma wF_0^2]^{1/2}$.

porphyrin and two axial benzylic E ligands (E = NMe_2) supplied by the EBrE donor groups of two adjacent zinc(II) porphyrins.

Two *trans*-positioned, *meso*-NBrN donor groups of each porphyrin take part in the intermolecular interactions between adjacent **1**Zn molecules. These are bent severely out of plane (see above). Only one CH_2NMe_2 donor functionality of these groups participates in bonding to an adjacent zinc atom. With respect to each other, these donor functionalities are positioned on opposite sides of the porphyrin plane (related to each other by the zinc inversion center). In the crystal structure, the other two NBrN donor groups (not shown in Figure 2) are mere spectator groups and do not participate in intermolecular bonding. They do, however, increase the symmetry of the molecules, which makes them statistically more prone to self-assembly (see below). The

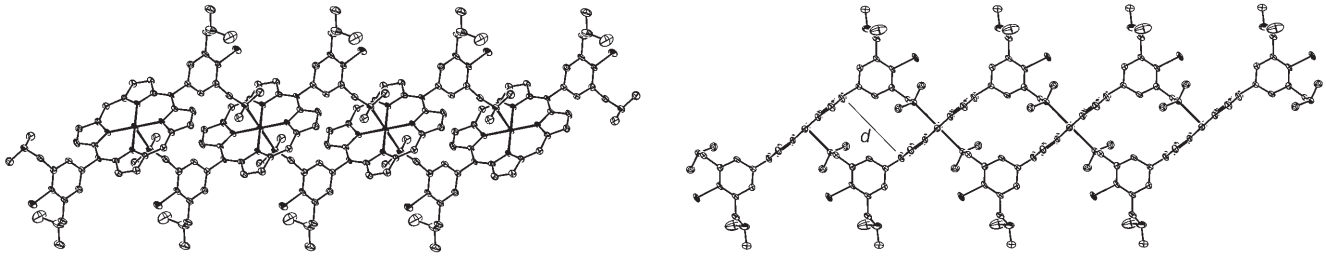

Figure 2. Two views of the one-dimensional polymer formed by **1**Zn, with thermal ellipsoids at 50% probability. Non-Zn-coordinating NBrN donor groups, solvent molecules, and hydrogen atoms are omitted for clarity. Left: part of the infinite, one-dimensional polymeric strand formed by **1**Zn. Right: view perpendicular to the porphyrin planes with interplanar distance *d* (see text).

porphyrins are aligned in a parallel manner, thus minimizing sterically unfavorable interactions between their substituents. Furthermore, they are displaced from a common axis to maximize zinc–heteroatom (Zn–N) interactions. Within the strands, one molecule of **1**Zn is repeated infinitely in an identical orientation and conformation. The axial Zn–N bond lengths are 2.564(4) Å, which is in the expected range for hexa-*N*-coordinate zinc(II) *meso*-tetraphenylporphyrins. For those hexa-*N*-coordinated complexes that have been crystallographically characterized to date, the axial N–zinc distances are in the range 2.467–2.490 Å for pyridine-type,[51–56] 2.470–2.552 Å for aniline-type,[51,52] and 2.473–2.520 Å for amine-type[57,58] Lewis bases.

In $[\mathbf{1}Zn]_\infty$, the phenyl groups connected to the coordinating N-donor groups are bent out of the porphyrin plane by 9.6(7)° towards the adjacent zinc porphyrin unit, whereas the other two *meso*-phenyl groups adopt a normal position with respect to the porphyrin ring. The *meso*-phenyl groups of the coordinating NBrN donors adopt dihedral angles of 75.9(8)° with the porphyrin; these angles are 57.4(4)° for the noncoordinating NBrN donor groups. The latter value is rather unusual and points to microenvironmental influence.[59] Within the polymeric strands, the Zn–Zn distances are 9.932(3) Å, with a distance between the least-squares planes of two adjacent porphyrins of 6.81(7) Å (*d* in Figure 2). Hence, the molecules are deviated from a common axis by 7.23 Å. Figure 3 shows the alignment of the individual polymer chains in the solid state. It reveals that identical polymer chains run in the same direction throughout the crystal and that the orientations of all the molecules are the same.

The three-dimensional features of the crystal structure of $[\mathbf{3}Zn]_\infty$ are virtually identical to those of $[\mathbf{1}Zn]_\infty$ (Figure 4). Also in this case, infinite polymer chains are formed through hexacoordination of zinc; axial Zn–O distances are 2.386(3) Å. Within the series of reported zinc(II) porphyrins with two axial O ligands,[51,52,60–71] this value is in the expected range for bis(ether) complexes. The Zn–O distances in bis(THF) complexes of ZnTPP derivatives are between 2.371[63] and 2.56 Å,[68] and in a zinc(II) porphyrin polymer the $Zn–O_{benzylmethylether}$ distances were found to be 2.434 Å.[72]

In the case of $[\mathbf{3}Zn]_\infty$, the phenyl groups connected to the coordinating EBrE donor groups (E = OMe) are bent out of the porphyrin plane by 13.7(8)° away from the adjacent zinc(II) porphyrin unit; this arrangement pulls two adjacent porphyrin rings closer together. The noncoordinating EBrE groups again adopt a normal geometry. As in the case of

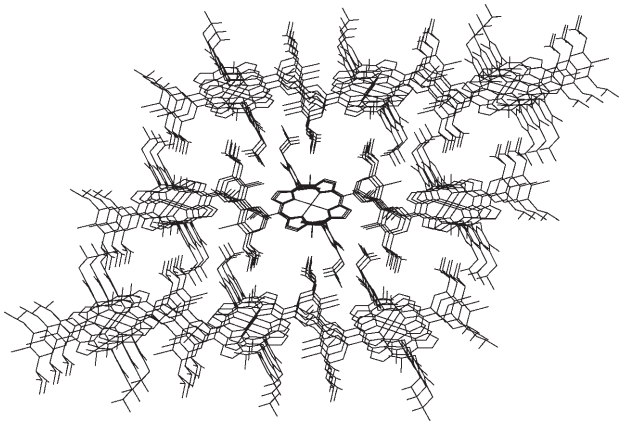

Figure 3. Stick-style representation of the 3D positioning of individual $[\mathbf{1}Zn]_\infty$ polymer strands in the crystal, shown along the axis running through the zinc(II) centers of the central strand.

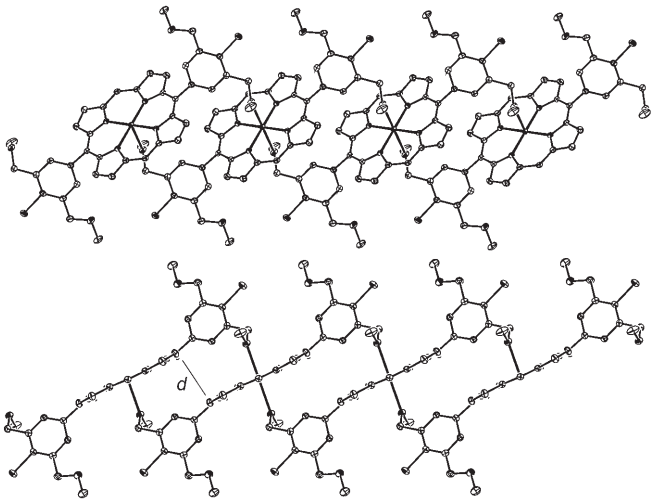

Figure 4. Two views of the one-dimensional polymers formed by **3**Zn with thermal ellipsoids at 50% probability. Nonbonding OBrO donor groups, solvent molecules, and hydrogen atoms are omitted for clarity. Top: part of the infinite, one-dimensional polymeric strand formed by **3**Zn. Bottom: view perpendicular to the porphyrin planes with interplanar distance *d* (see text).

$[\mathbf{1}Zn]_\infty$, the interplanar angles of the coordinating and noncoordinating OBrO donor groups with respect to the porphyrin ring are quite distinct: 65.8(3)° for the coordinating groups versus 75.8(2)° for the noncoordinating groups. The Zn–Zn distances in the polymer strands in $[\mathbf{3}Zn]_\infty$ are 8.7503(8) Å, whereas the distance *d* between the least-square planes through the pyrrolic nitrogen atoms of two juxtaposed porphyrins is 3.47(10) Å (Figure 4), which places the porphyrins 8.03 Å from a common axis. Unfortunately, we were not able to obtain single crystals of **2**Zn and **4**Zn. The NMR and UV/Vis spectra, however, suggest the existence of similar intermolecular interactions as in $[\mathbf{1}Zn]_\infty$ and $[\mathbf{3}Zn]_\infty$ (see below).

The polymeric solid-state structures formed by self-assembly of **1**Zn and **3**Zn are rather unusual in that they feature hexacoordination of the zinc(II) atoms, which usually prefer pentacoordinate, distorted-square-pyramidal ligand environments in porphyrins. To investigate whether the hexacoordination is imposed by the nature of the ERE donor groups (R = H or Br) or is a consequence of the predisposition of Lewis basic and acidic moieties within the molecules, we studied the structural features of coordination complexes of the various constituents of the tetrakis(ERE donor) zinc(II) porphyrins. We first set out to crystallize 2-[(dimethylamino)methyl]bromobenzene (DMBABr), *N,N*-dimethylbenzylamine (DMBA), 2-methoxymethylbromobenzene (MBEBr), and methylbenzylether (MBE) adducts of ZnTPP (Scheme 3).

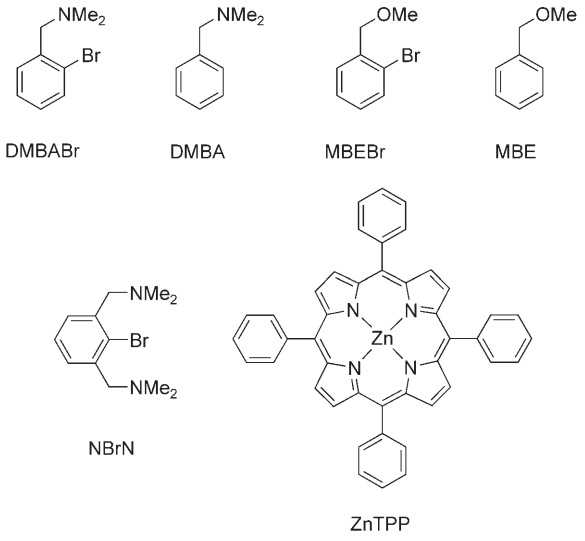

Scheme 3. Model compounds.

Crystallizations were set up by using 8 equivalents of the respective Lewis base per molecule of ZnTPP, so as to imitate the Lewis acid/Lewis base ratio present in solutions of **1**Zn–**4**Zn. The starting materials were dissolved in CH_2Cl_2 and the respective solutions were layered with hexane, after which they were allowed to concentrate slowly by evaporation.

In the case of DMBABr–ZnTPP and DMBA–ZnTPP, large block-shaped crystals grew in essentially quantitative yields with respect to ZnTPP. The crystal structures of DMBABr–ZnTPP and DMBA–ZnTPP have common molecular features, and the filling of the unit cell is similar (Table 1). Both compounds crystallize as 1:1 adducts of the zinc porphyrin and the amine, in which five nitrogen atoms form a distorted-square-pyramidal ligand environment around the zinc atom (Figure 5, top). The four pyrrolic nitrogen atoms of the porphyrin form the base of the pyramid, and the apical, fifth ligand position is occupied by the benzylic N5 atom of either the DMBABr or the DMBA ligand. The zinc atoms are dislocated 0.3344(2) and 0.33158(18) Å from the porphyrin least-squares plane towards the apical ligand, respectively. In DMBABr–ZnTPP, the $Zn–N_{pyrrole}$ bond lengths are in the range 2.0566(18)–2.0708(16) Å, whereas in the case of DMBA–ZnTPP, these bond lengths are in the range 2.0611(13)–2.0695(13) Å. The $Zn–N_{apical}$ bond lengths, at 2.2254(13) and 2.23661(17) Å, respectively, are also comparable. In both cases, the C3–N5 bond is almost colinear with the N1–Zn–N2 vector, with a dihedral angle of −14.42(14)° for DMBABr–ZnTPP and −13.58(12)° for DMBA–ZnTPP. Although the similarities between both structures are clear, the steric bulk of the *ortho*-Br atom causes a tilt in the phenyl ring of the DMBABr ligand with

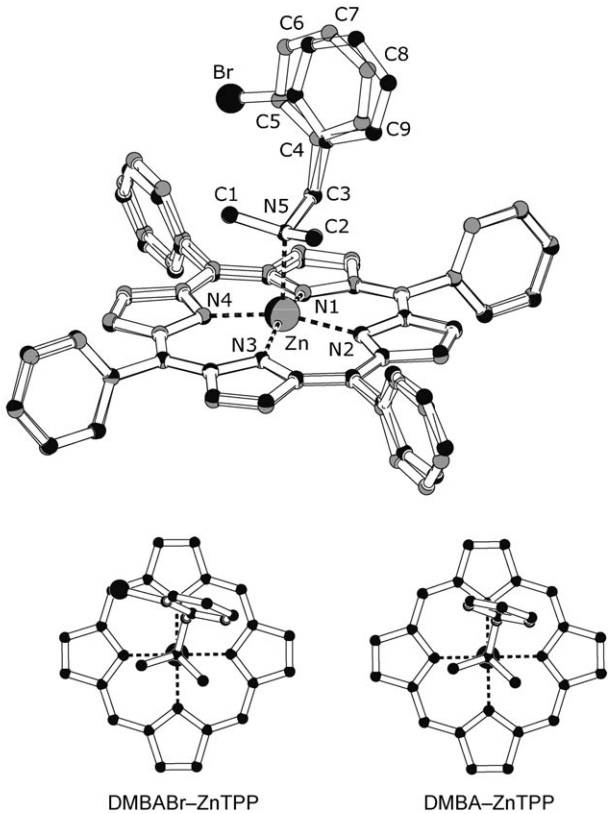

Figure 5. Quaternion fit overlay plot (top) of DMBABr–ZnTPP (black) and DMBA–ZnTPP (gray), in which the hydrogen atoms are omitted for clarity. The views along the N5–Zn vector of each compound are depicted below without the *meso*-phenyl rings.

respect to the porphyrin plane by virtue of rotation around the N5–C3 bond. The Zn–N5–C3–C4 torsion angle is −172.71(15)° for DMBABr–ZnTPP compared to −179.29(13)° for DMBA–ZnTPP. The angle between the porphyrin plane and the phenyl ring of the ligand is also influenced by the bromine atom. For DMBABr–ZnTPP, the interplanar angle is, at 78.80(9)°, smaller than in the case of DMBA–ZnTPP, in which it is 81.25(8)° (Figure 5, bottom).

In spite of numerous attempts, the crystals that formed from solutions of ZnTPP (1 equiv) and MBE or MBEBr (each 8 equiv) invariably did not contain MBE or MBEBr, respectively. When wet solvents were used, H_2O–ZnTPP was formed quantitatively (Figure 6 and Table 1).[73] Apparently, H_2O is a better ligand for the central zinc(II) atom than a benzylic oxygen atom. This is for steric rather than inherent Lewis basic reasons, as a dialkyloxide is expected to be a stronger Lewis base than dihydrogenoxide.

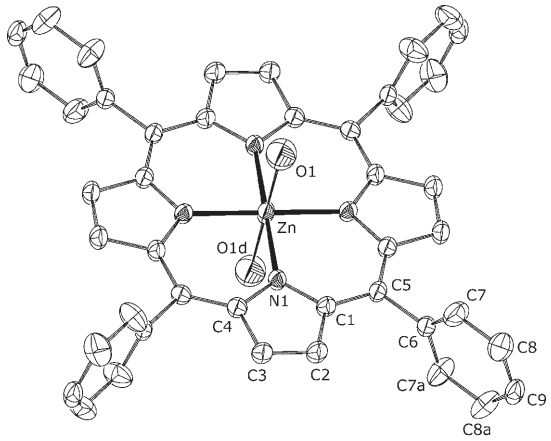

Figure 6. Crystal structure of H_2O–ZnTPP with thermal ellipsoids at 50% probability. Hydrogen atoms are omitted for clarity. The oxygen atom has a 50% occupancy on either side of the porphyrin plane. Relevant bond lengths (Å) and angles (°): Zn–N 2.035(2), Zn–O 2.369(9); N1-–Zn–N1a 90.00(10), N1–Zn–N1b 180.0, N1–Zn–O1 90.00.

In a further experiment, crystals were grown from a mixture of ZnTPP and 4 equivalents of NBrN, in which the same ratio of NBrN groups and zinc(II) porphyrin building blocks was present as in **1**Zn. The crystals that were formed quantitatively (with respect to ZnTPP) consisted of NBrN–$(ZnTPP)_2$ (Figure 7 and Table 1). In this supramolecular assembly, two parallel ZnTPP molecules, the least-squares planes of which are separated by 10.498(7) Å, are connected by one molecule of NBrN, which functions as a bidentate bridging group through its two benzylic nitrogen atoms N5 and N5a. The two pentacoordinate zinc atoms are 10.8033(7) Å apart, and there is an inversion center at half this distance, leading to a centrosymmetric system. As with DMBABr–ZnTPP and DMBA–ZnTPP, the zinc atoms are displaced from the least-squares planes created by the four pyrrolic nitrogen atoms of the porphyrin by 0.3548(2) Å towards the apical amine ligands. The Zn–N5 and Zn–N5a

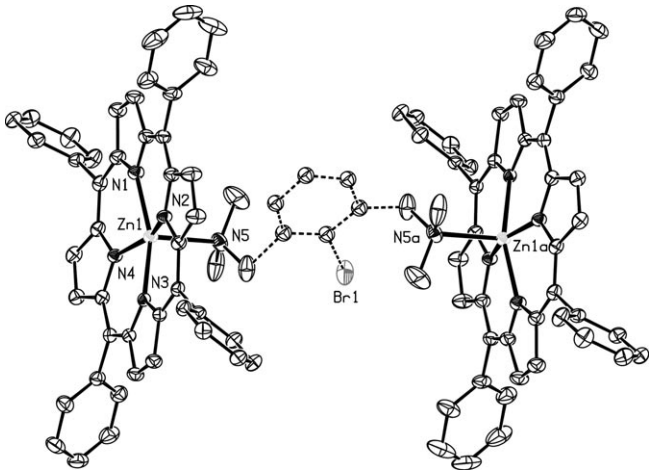

Figure 7. Molecular structure of NBrN–$(ZnTPP)_2$ with thermal ellipsoids at 50% probability. Hydrogen atoms are omitted for clarity. Only one disordered form of the central ligand is shown. Symmetry code: $a = 1-x$, $-y$, $-z$.

distances are 2.263(2) Å. The bridging NBrN ligand can apparently adopt two different conformations in the solid state, and each of them can be rotated by 180° along the axis through the two benzylic carbon atoms. Hence, the central NBrN unit is fourfold disordered (Figure 7).

Solid-State UV/Vis Spectroscopy

Solid-state UV/Vis spectra were recorded of samples of **1**Zn–**4**Zn (Figure 8). The reference compound {tetrakis[3,5-bis(*tert*-butyl)phenyl]porphyrinato}zinc(II) (**5**Zn) showed a strong absorbance at 430 nm (Soret band), as well as two Q bands at 549 and 587 nm, the intensity ratio of which was 4.91 (A_{549}/A_{587}). The solid-state spectra of **2**Zn and **4**Zn are very similar to those of the crystallographically characterized compounds **1**Zn and **3**Zn. With respect to the spectrum of **5**Zn, the Soret bands of **1**Zn–**4**Zn exhibited a red shift of 4 to 9 nm (Table 2). Both Q bands of each tetrakis(ERE donor) zinc(II) porphyrin were also shifted bathochromically relative to the Q bands of **5**Zn. Furthermore, the intensity

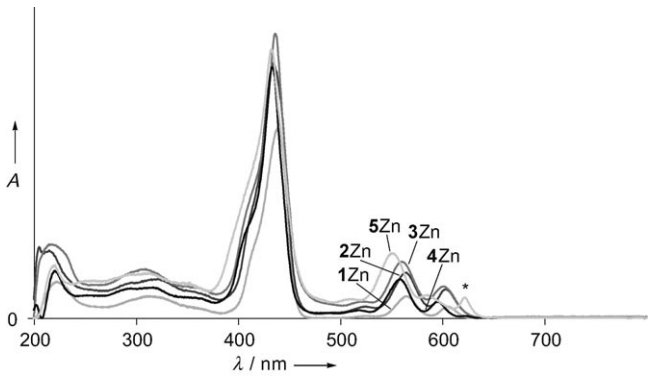

Figure 8. Solid-state UV/Vis spectra of **1**Zn–**4**Zn. The peak at around 620 nm for **5**Zn (*) corresponds to chlorine impurity in the sample.

Table 2. Absorption maxima of the solid-state UV/Vis spectra of ***n*Zn**.

Compound	Soret [nm] (I_{rel})	Q_{vib} [nm] (I_{rel})	Q (I_{rel})
1Zn	439 (1.000)	565 (0.115)	606 (0.060)
2Zn	438 (1.000)	564 (0.126)	604 (0.060)
3Zn	438 (1.000)	560 (0.163)	601 (0.075)
4Zn	434 (1.000)	558 (0.155)	596 (0.065)
5Zn	430 (1.000)	549 (0.134)	587 (0.027)

ratio between the two Q bands was lowered to 1.9–2.4 (Table 1), which is indicative of ligand binding to the zinc centers. A slight bathochromic shift was also observed when going from **2**Zn and **4**Zn to **1**Zn and **3**Zn (from R = H to R = Br), and when going from **3**Zn and **4**Zn to **1**Zn and **2**Zn (from O coordination to N coordination).

Solution UV/Vis Spectroscopy

Solution UV/Vis spectra of **1**Zn–**4**Zn were recorded at room temperature in CH_2Cl_2. The concentrations were varied between 0.11 and 50 μM. The spectra of **2**Zn showed a Q-band region indicative of pentacoordinate zinc(II) porphyrins (Figure 9, bottom). The high-energy Q band at $\lambda = 562$ nm (Q_{562}) is accompanied by a lower-energy band at $\lambda = 602$ nm (Q_{602}). The intensity ratio (A_{562}/A_{602}) amounts to about two, which points to coordination of an apical nitrogen atom to zinc.[74] Throughout the entire concentration range, both the peak positions and intensities did not change, which indicates a strong association constant (K_{ass}) (Figure 9, bottom).

At high concentrations, the spectra of **1**Zn (R = Br) are very similar to those of **2**Zn (R = H), with Q bands at $\lambda =$ 562 and 603 nm ($A_{562}/A_{603} = 1.9$). In this case, however, the Q-band region does change upon lowering the concentration. At concentrations less than 7 μM, Q_{562} clearly started to broaden and shifted hypsochromically to 553 nm at 0.11 μM. The intensity of Q_{603} concomitantly dropped to give a final intensity ratio (A_{553}/A_{603}) of 3.6 (Figure 9, top). This change indicates that, at lower concentrations, fewer zinc(II) centers remain coordinated to the NBrN donor groups, that is, the intermolecular interactions between molecules of **1**Zn are weaker than those between molecules of **2**Zn.

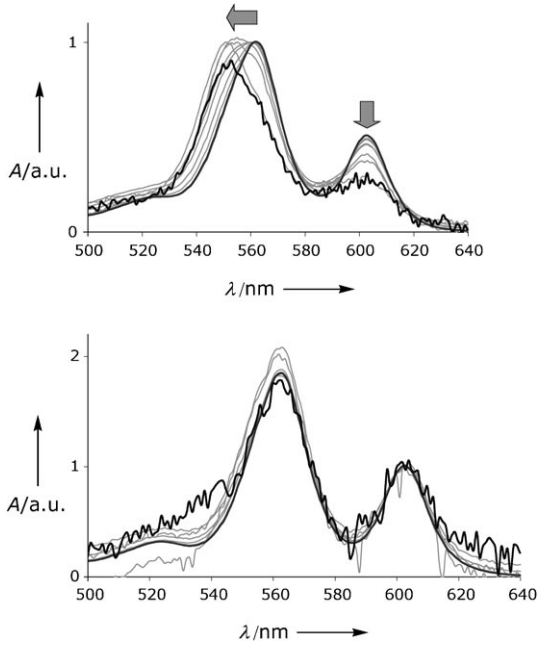

Figure 9. Concentration dependence of the Q-band region of the UV/Vis spectra of **1**Zn (top) and **2**Zn (bottom) in CH_2Cl_2 at room temperature. For **1**Zn, the arrows indicate the effect of dilution of the sample.

The spectra of **3**Zn and **4**Zn recorded in the same concentration range did not show evidence for the existence of intermolecular interactions; the spectra were indicative of tetracoordinate zinc(II) porphyrins. Addition of a large excess of THF, however, clearly led to the coordination of THF to the zinc centers as judged by UV/Vis spectroscopy.

To gain further insight into the supramolecular chemistry of the tetrakis(ERE donor) zinc(II) porphyrins, the stability constants of simple model combinations of DMBABr, DMBA, MBEBr, and MBE with ZnTPP were also determined. To assess the strength of the Zn–N and Zn–O bonds in these combinations, the K_{ass} values in CH_2Cl_2 were determined by means of UV/Vis spectroscopic titrations. Solutions of ZnTPP in CH_2Cl_2 (≈1 μM) were titrated with the relevant ligand (>100 equiv), and the absorbances at two wavelengths (422 nm for the tetracoordinate nonligated ZnTPP and 427 nm for the pentacoordinate ligated complex) were monitored and analyzed with Benesi–Hildebrand plots (see Experimental Section).[75] For each combination of ZnTPP and Lewis base, an isosbestic point was observed, which indicates a single equilibrium between the two species, and the binding curves were fitted to a 1:1 model with excellent results. In the case of the amine ligands, it was found that the association constants with ZnTPP ($K_{ass} \approx 2100\ M^{-1}$ for DMBA and $1200\ M^{-1}$ for DMBABr) were significantly lower than those for pyridine ($K_{ass} \approx 7720\ M^{-1}$) or benzylamine ($K_{ass} \approx 12\,000\ M^{-1}$).[76] In the latter case, the increase in Lewis basicity (as a σ donor) when going from primary to tertiary amine is most probably overruled by the increase in steric bulk around the nitrogen atom in the DMBA and DMBABr ligands.[77] The benzylic ether functionalities, on the other hand, bind much more weakly to the zinc atoms in dry CH_2Cl_2: for MBE, a K_{ass} values of about $5\ M^{-1}$ was found, and in the case of MBEBr, no association constant could be determined.

^{1}H NMR spectroscopy

As the UV/Vis spectra of **1**Zn and **2**Zn showed aggregation of the molecules in solution at low concentrations, but could not provide additional information as to how the oligomeric or polymeric structures are organized in solution, solutions of these compounds were investigated by ^{1}H NMR spectroscopy at various temperatures (Figure 10).

The ^{1}H NMR spectra (300 MHz) of both **1**Zn (R = Br) and **2**Zn (R = H) at room temperature consist of broad peaks for all resonances. The spectrum of **1**Zn at 298 K

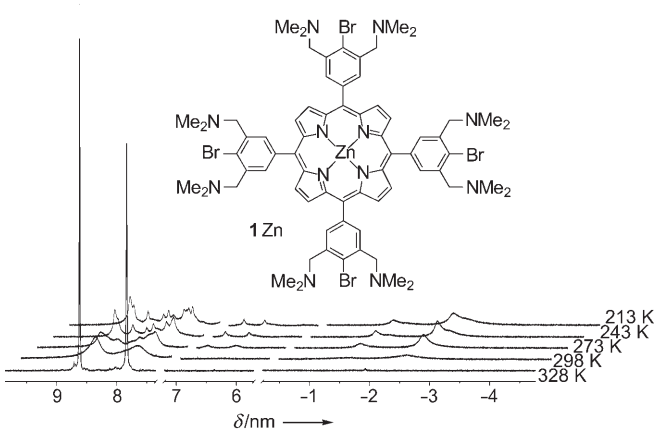

Figure 10. Aromatic and shielded aliphatic regions of the ^{1}H NMR spectra of **1**Zn at different temperatures.

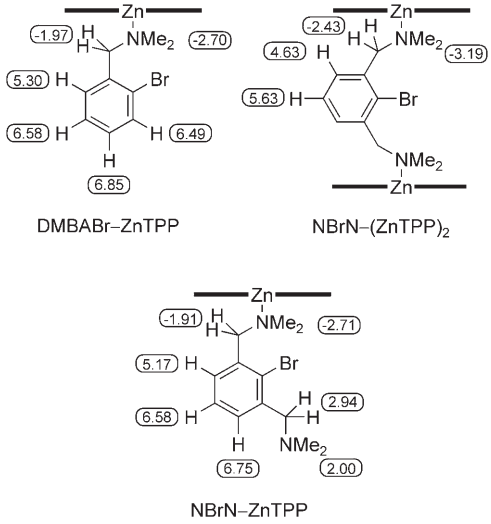

Figure 11. ^{1}H NMR chemical shifts of the protons of the nitrogenous ligands in DMBABr–ZnTPP, NBrN–$(ZnTPP)_2$, and NBrN–ZnTPP at 213 K in $CDCl_3$.

shows four broad signals centered around $\delta = 8.56$ (8H; β-H), 7.78 (8H; ArH), 3.24 (16H; CH_2N), and 1.90 ppm (48H; $N(CH_3)_2$) (Figure 10), whereas the spectrum of **2**Zn consists of five broad signals at $\delta = 8.61$ (8H; β-H), 7.67 (8H; ArH), 7.20 (4H; ArH), 2.92 (16H; CH_2N), and 1.74 ppm (48H; $N(CH_3)_2$). The extent of line broadening was most pronounced for the signals of the benzylic and dimethylamino protons, whereas the signals of the β-protons were broadened the least. In both complexes, the signals of the benzylic (CH_2NMe_2) and dimethylamino ($CH_2N(CH_3)_2$) protons in particular were shifted rather drastically with respect to those of their parent, free-base porphyrins. When compared to the spectra of **1** and **2**, these signals had shifted to higher field by 0.80 and 0.61 ppm in the former case and by 0.83 and 0.71 ppm in the latter. Both room-temperature spectra did not show concentration dependence within the concentration range 1–15 μM. Addition of an excess of [D_5]pyridine led to a sharpening of all signals with concomitant shifts to normal values for discrete molecular pyridine–zinc(II) porphyrin assemblies. When solutions of **1**Zn and **2**Zn were heated to 328 K, all the signals also sharpened, thus pointing to the dynamic coordination/dissociation of the molecules in solution (Figure 10).

Next, ^{1}H NMR spectra were recorded at lower temperatures. For reasons of comparison and peak assignment, the ^{1}H NMR spectra of DMBABr–ZnTPP, NBrN–$(ZnTPP)_2$, and NBrN–ZnTPP were recorded (see Figure 11 and Experimental Section). Upon cooling, the four signals of **1**Zn initially broadened even further, but gradually more peaks emerged (Figure 10). At 288 K, signals emerged at $\delta = -1.31$ and -2.24 ppm, which are ascribed to the benzylic and dimethylamino protons next to the nitrogen atoms coordinated to neighboring zinc atoms. The spectrum recorded at 266 K also showed additional peaks in the aromatic and benzylic regions. Two signals of equal intensity were observed at $\delta = 7.05$ and 6.55 ppm (ascribed to ArH on an NBrN donor group coordinated through one amine arm), and, concomitantly, peaks emerged at $\delta = 3.10$ and 2.20 ppm. The latter most probably belong to the benzylic and dimethylamino protons next to a noncoordinating nitrogen atom, which are on a benzene ring to which the other amine arm is coordinated ($\delta = 2.94$ and 2.00 ppm, respectively for the corresponding protons in the case of NBrN–ZnTPP; Figure 11). At 218 K, **1**Zn showed splitting of all peaks into multiplets. Numerous, mutually overlapping aromatic signals were visible, although they remained quite broad (Figure 10). In the benzylic region of the spectrum, three separate signals were present: a broad signal at $\delta \approx 3.71$ ppm (12H) consisting of a few unresolved peaks, a signal at $\delta =$ 3.01 ppm (2H), and a signal at $\delta = -1.54$ ppm (2H); these signals support the formation of a 1:1 complex of (the nitrogen atom of) one molecule of **1**Zn with (the zinc atom of) another molecule of **1**Zn. The low-temperature ^{1}H NMR spectroscopic behavior of **2**Zn was found to be similar to that of **1**Zn, but the spectra were more complex. For both **3**Zn and **4**Zn, the ^{1}H NMR spectra showed sharp peaks for all resonances at room temperature. These peaks, however, were slightly shifted to higher field relative to **3** and **4**, which indicates an equilibrium between tetra- and pentacoordinate zinc(II) porphyrins that strongly prefers the former. Upon cooling solutions of **3**Zn and **4**Zn to 211 K, the peaks broadened and shifted upfield, but no splitting or fine structure was observed.

Discussion

Hexacoordinate Zinc(II) Centers

Zinc(II) ions incorporated in porphyrin systems generally prefer a four-coordinate, square-planar or five-coordinate, distorted-square-pyramidal coordination environment.[78] It was recognized that octahedrally coordinated zinc(II) porphyrins can be formed as well,[51–56,61–71] especially when the

porphyrin ligand bears multiple electron-withdrawing groups.[57,60,79] Hexacoordination at zinc can also be caused by the presence of an excess of ligand that is not covalently connected to the zinc(II) porphyrin,[56] for example, solvent. Recently, it was found that by carefully designing zinc(II) porphyrin monomers, a three-dimensional coordination polymer could be formed via six-coordinate zinc(II) with two axial oxygen donors.[72] Compounds **1**Zn–**4**Zn presented herein all contain eight Lewis basic sites and, in principle, one Lewis acidic site (the zinc atom). This makes the formation of supramolecular aggregates through coordination bonds possible. Their crystal structures indeed show that **1**Zn and **3**Zn self-aggregate to form one-dimensional infinite coordination polymer strands, $[\mathbf{1}Zn]_\infty$ and $[\mathbf{3}Zn]_\infty$. Surprisingly, the zinc atoms at the porphyrin centers are not penta- but hexacoordinate. In the present case, hexacoordination at zinc is imparted by the unique combination of Lewis basic and acidic sites within the tetrakis(ERE donor) zinc(II) porphyrins (E = NMe_2, OMe; R = Br, H) in combination with their mutual spatial predisposition. In fact, there is an excess of ligand. Furthermore, the crystal structures of DMBABr–ZnTPP, DMBA–ZnTPP, and NBrN–$(ZnTPP)_2$ show that the hexacoordination of zinc is not dictated by the inherent properties of the *N,N*-dimethylbenzylamine ligand fragment. No evidence was found for hexacoordination of the zinc(II) ions in these model systems in solution.

Influence of Br Atoms

UV/Vis titrations showed that the bromine atoms in DMBABr and MBEBr significantly lower the coordination strengths of DMBA and MBE, respectively, toward ZnTPP. Because the through-bond inductive effects of the bromine atom are anticipated to be negligible, the intrinsic Lewis basicity of the benzylic nitrogen atoms in both cases is expected to be identical. Comparison of the crystal structures of DMBABr–ZnTPP and DMBA–ZnTPP provides some indications as to why the DMBA ligand binds much more strongly to ZnTPP than DMBABr does. In the crystal structures, the difference in association constant between DMBABr and DMBA is indicated by the larger tilt of the DMBABr phenyl ring with respect to the porphyrin plane (Figure 5). Furthermore, space-filling models show a repulsion between the porphyrin macrocycle and the rather large bromine atom. The effect of the *ortho*-Br atom in our systems is comparable to the effect found by Mizutani et al.[76] They found that the K_{ass} values of $PhCH_2NH_2$ and $PhCH_2CH_2NH_2$ with ZnTPP are 12000 and 46000 M^{-1}, respectively; however, their pK_a values are not that different (9.00 vs. 9.96). A similar steric effect on K_{ass} was observed for tBuNH$_2$ and nBuNH$_2$; here, the pK_a values are very similar (11.44 and 11.48), but the K_{ass} values with ZnTPP differ significantly (14000 and 40000 M^{-1}, respectively). The difference between the coordination strengths of MBEBr and MBE toward ZnTPP is likely to be caused by the same steric factor.

The effect of the *ortho*-bromine atoms on the binding constants of *N,N*-dimethylbenzylamine to zinc porphyrin also seems to have a pronounced effect on the stability of the coordination polymers formed by **1**Zn–**4**Zn. Dilution UV/Vis experiments showed a concentration dependence of the spectra of **1**Zn, whereas the spectra of **2**Zn remained unaffected throughout the concentration range investigated. These observations illustrate nicely the increased stability of the coordination dimers/oligomers devoid of bromine substituents on their ERE donor groups.

Self-Assembly

Subtle variations of the structural parameters of Lewis base substituted zinc(II) tetraphenylporphyrins can lead to completely different self-assembly behavior. This is illustrated by a comparison of the structure of $[\mathbf{3}Zn]_\infty$ with the supramolecular polymers reported by Lai and co-workers.[72] Although the central metal (Zn) and the number (two) and nature ($ArCH_2OMe$) of coordinating heteroatoms are identical, the differences in the positions of the methoxymethyl groups (*ortho* in the systems of Lai and co-workers as opposed to *meta* in **3**Zn and **4**Zn) and the number of phenyl groups around the porphyrin (two as opposed to four) leads to an entirely different supramolecular organization in the solid state. In this respect, a few important conclusions can be drawn from the crystal structures of $[\mathbf{1}Zn]_\infty$ and $[\mathbf{3}Zn]_\infty$. First, a change in the benzylic heteroatoms does not result in a change in the overall mode of self-assembly (one-dimensional, cofacial polymers). This change, however, affects the distance between the Zn and E atoms, which, in turn, changes several structural parameters such as separation of the porphyrin planes, slippage of the porphyrin planes from a common axis, and Zn–Zn distances. Besides variation of the benzylic heteroatoms, substitution of the *meso*-phenyl rings at a position *para* with respect to the porphyrin ring may further steer the intricate structural parameters of the polymers. The mere presence of a Br atom changes the way in which the *N,N*-dimethylbenzylamine ligand binds to ZnTPP (Figure 5). This may also affect the solid-state structures of **2**Zn and **4**Zn relative to those of **1**Zn and **3**Zn.

The combined presence of Lewis acidic and basic sites within a single molecule leads to the formation of polymers by **1**Zn–**4**Zn. The spatial predisposition of these Lewis acidic and basic sites, however, seems to play a crucial role in determining the structure of the polymers formed. It is apparent from Figures 2 and 4 that the benzylic heteroatoms that participate in the assembly process are supplied by two ERE donor groups, which are positioned *trans* (at C5 and C15) with respect to each other on the porphyrin ring. The coordinating heteroatoms themselves are located on opposite sites of the porphyrin plane. Importantly, both factors are always guaranteed by the present systems. Because of this, the way in which two monomers approach each other during crystallization is always "correct" and statistically favorable for the formation of the polymers. In other words,

every molecular encounter leads to a matching situation on the way to polymer formation.

Whereas the polymeric structures of **1**Zn and **3**Zn in the solid state were proved by X-ray crystallography, the solid-state structures of **2**Zn and **4**Zn, unfortunately, could not be solved, despite numerous crystallization attempts. Their solid-state UV/Vis spectra, however, show substantial similarities to the spectra obtained from **1**Zn and **3**Zn. The data obtained from NMR spectroscopy also support the assumption that their structures are comparable.

In considering the formation of the coordination polymers, we propose a step-wise mechanism in which dimers are first formed and polymerization proceeds through the interaction of the dimers. Initially, a zinc atom of one molecule has to interact with a peripheral heteroatom, O or N, of a second molecule. Once this bond is formed, the zinc atom of the second molecule will bind, now through an intramolecular coordination event, to a peripheral heteroatom of the former to form a coordination dimer (Figure 12).

The association constant of this dimer, estimated at about $1\times10^{9}\,\text{M}^{-1}$,[80] is much larger than the sum of the association constants of the two Zn–N bonds.[81] The formation of dimers is inferred from the dilution experiments shown in Figure 9. Even at high dilution (down to 0.1 μM), the UV/Vis spectra of **1**Zn and **2**Zn still show coordination saturation at zinc (pentacoordination). The strength of one bond between monomers (with K_{ass} of 1200 or $2100\,\text{M}^{-1}$, respectively) is not strong enough to account for this behavior. The high association constants of these dimers are largely due to the simultaneous binding of the two sides. It may, however, also contain an extra entropic term, which takes into account the fact that when one Zn–N bond breaks, there are still three identical N donor groups on the same side of the porphyrin available for bonding by virtue of rotation around the intact Zn–N bond.[82]

An increase in dimer concentration results in interactions between them (Figure 13), which ultimately leads to polymers. One could assume that, at intermediate concentrations, only pentacoordinate Zn centers exist and that, there-

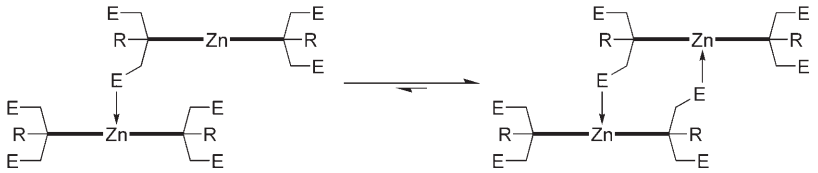

Figure 12. Formation of an ***n***Zn dimer in solution through intramolecular coordination. Only the four E donor sites in each plane are shown.

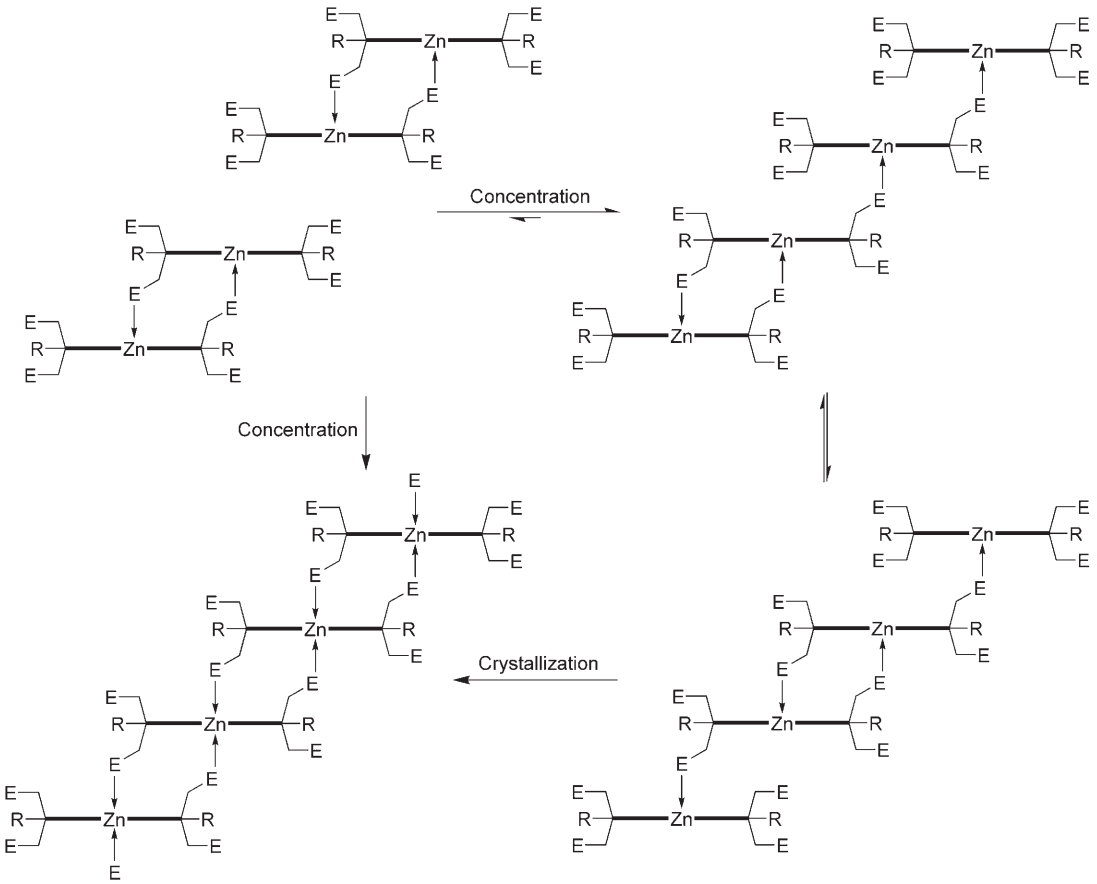

Figure 13. Proposed mechanisms for oligomerization of ***n***Zn dimers in solution, eventually leading to the one-dimensional polymers $[\boldsymbol{n}\text{Zn}]_{\infty}$ in the solid state.

fore, the interaction between dimers takes place with a concomitant making of interdimer and breaking of intradimer coordination bonds (Figure 13, right). The final polymer is then generated by formation of hexacoordinate zinc centers in the last (crystallization) step only. Alternatively, the relative stability of the dimers could lead to a one-step oligomerization and polymerization event, in which interdimer interactions immediately take place through the formation of hexacoordinate zinc centers (Figure 13, left).

At higher concentrations, the ^{1}H NMR spectra confirmed supramolecular aggregation between the ***n*Zn** molecules. Broad signals observed at room temperature were split into several signals at lower temperatures, which suggests the existence of oligomeric structures. These spectra unfortunately did not provide a detailed picture of the structures in solution and of the extent of oligo/polymerization. Preliminary static and dynamic light scattering (SLS, DLS) measurements performed at high and low concentrations showed that structures with hydrodynamic radii larger than 10 nm were not present. These observations corroborate the idea that dimers are the predominant species at low concentration, whereas oligomers may be present at higher concentration. The latter, however, do not have a high degree of oligomerization.

Relevance to Biological Systems

Nature uses cyclic and linear polymeric porphyrin assemblies to harvest light energy from the sun. The cyclic structures of the RC-LH1[6,83] and LH2[4] complexes (RC = reaction center, LH = light-harvesting core), which are used by certain purple bacteria, have been elucidated by X-ray crystallography. The way in which bacteriochlorophyll (BChl) molecules self-assemble to form the light-harvesting complexes found in the chlorosomes of green sulfur bacteria, however, remains a subject of debate in the absence of X-ray crystallographic evidence. In particular, Tamiaki and coworkers[8,84–87] and Balaban et al.[7,88–90] have put much effort in devising (semi-)synthetic mimics of self-assembling BChl units to investigate the self-assembling structures. Balaban recently made a very convincing case for a model, in which BChl monomers are assumed to self-assemble through intermolecular interactions between the central magnesium atom of one BChl molecule, the ketone oxygen atom of one of its BChl neighbors, and the hydroxy oxygen atom of the other neighbor (Figure 14, right).[7]

This structural model is based on the self-assembly behavior of the synthetic mimic **6**Zn (Figure 14), as evidenced by X-ray crystallography. Given the structural and physicochemical similarities between **6**Zn and the molecules nature uses in its chlorosomes, the supramolecular structures of the self-assembled chlorosome structures were believed to resemble closely the crystal structure of **6**Zn (Figure 14).

Even though the zinc(II) porphyrins reported herein do not closely resemble the natural BChl chromophores on a molecular level, the supramolecular structures they form in the solid state are to a large extent structurally analogous to the self-assembled natural systems suggested by Balaban. The porphyrin macrocycles are cofacially aligned, the central metal atoms are ligated by two axial donor atoms located on opposite sides of the neighboring porphyrin rings, and the interplanar distances of 3.5 and 6.8 Å for $[\mathbf{3}Zn]_\infty$ and $[\mathbf{1}Zn]_\infty$, respectively, are very similar to the interplanar distances of 3.3–3.5 Å proposed for the natural systems. Important structural parameters for the functions of the chlorosomes are the distances between the planes of the tetrapyrrolic macrocycles as well as their center-to-center distances. At the moment, there is a shortage of methods to vary systematically these key factors in synthetic systems, which may actually be quite relevant for the investigation of their importance. Herein, we have shown that some important structural parameters of simple synthetic porphyrin polymers that structurally resemble the natural systems can be readily tuned by variation of the Lewis basic heteroatoms at the porphyrin periphery without disrupting the one-dimensional, cofacial polymeric structure. These factors are probably also influenced by other variations in the porphyrin substitution pattern, such as the ERE donor R group (R = H, Br) in this work.

Conclusions

Tetrakis(ERE donor) zinc(II) porphyrins **1**Zn–**4**Zn have been synthesized in excellent yields by selective zinc(II) introduction in the corresponding hybrid ligands. As these zinc(II) porphyrins comprise one Lewis acidic and eight

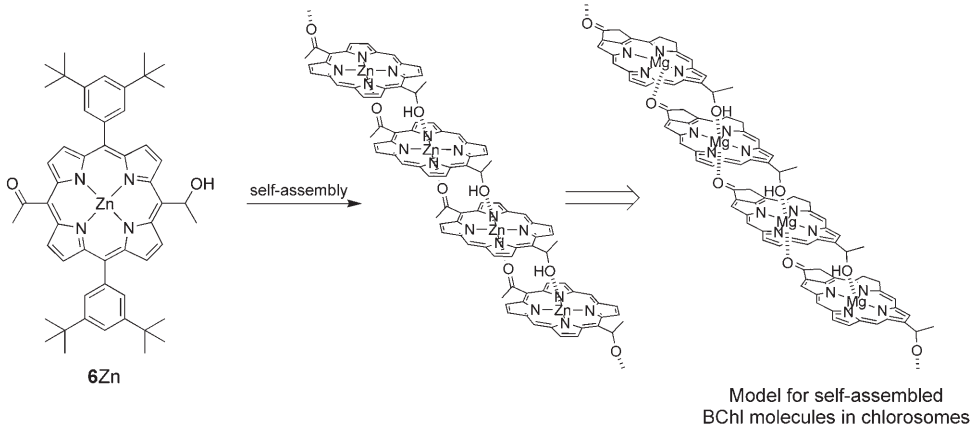

Figure 14. Proposed structure of the BChl aggregates in chlorosomes on the basis of the self-assembly behavior of model compound **6**Zn. In the depictions of the polymers, other ring substituents are omitted.

Lewis basic sites, they self-aggregate to form one-dimensional polymers in the solid state, as exemplified by the crystal structures of $[\mathbf{1}Zn]_\infty$ and $[\mathbf{3}Zn]_\infty$. These polymers consist of cofacially aligned [tetrakis(ERE donor)porphyrinato]zinc(II) molecules, which are mutually connected through hexacoordinate zinc atoms. On the basis of a combination of solution-phase experiments, we propose that these polymers are produced through the initial formation of dimers followed by dimer polymerization at high concentration. Furthermore, it was concluded from these experiments that, although supramolecular interactions beyond the dimer structure do exist, the degree of polymerization in solution is low.

These systems provide an attractive new entry for the construction of supramolecular multiporphyrin arrays that are of interest in relation to several biological light-harvesting complexes. Given the modularity of a number of structural parameters of these porphyrins (benzylic heteroatoms E, aryl substituent R, and porphyrin metal), they represent an interesting addition to the limited number of synthetic porphyrin derivatives capable of forming chlorosome-like structures. The photophysical properties of such compounds are currently under investigation.

Experimental Section

General

All reactions were performed under dry nitrogen atmosphere with standard Schlenk techniques and were shielded from ambient light with aluminum foil. CH_2Cl_2 was distilled from CaH_2. MeOH was degassed before use by bubbling dry N_2 through it for at least 20 min. All standard reagents were purchased from ACROS Organics and used as received. The synthesis of compounds **2** and **4** has been published,[45] and the synthesis of **1** and **3** will be described shortly.[47] DMBABr,[91] MBEBr,[92] and ZnTPP[93] were prepared according to literature procedures. $CDCl_3$ for NMR spectroscopy was distilled from CaH_2 and stored in the dark. Samples for ^1H and $^{13}C\{^1H\}$ NMR spectroscopy were dissolved in $CDCl_3$ and recorded at 300 and 75 MHz, respectively, on a Varian 300 spectrometer operating at 298 K. Resonances were referenced to residual solvent signals ($\delta_H = 7.26$ ppm for $CHCl_3$ in $CDCl_3$; $\delta_C = 77.16$ ppm (central peak) for $CDCl_3$). UV/Vis spectra were recorded on a Cary 50 UV/vis spectrophotometer, and solid-state UV/Vis spectra were recorded with KBr mixtures on a Varian Cary 5 UV/Vis/near-IR spectrophotometer. MALDI-TOF measurements were performed on an Applied Biosystems Voyager-DE PRO biospectrometry workstation with 2,5-dihydroxybenzoic acid as matrix. ESI-MS measurements were performed at the Biomolecular Mass Spectrometry Group, Bijvoet Centre for Biomolecular Research, Utrecht University, The Netherlands. Elemental microanalysis was performed by Dornis und Kolbe, Mikroanalytisches Laboratorium, Müllheim a/d Ruhr, Germany.

Syntheses

1Zn: A dark-red solution of **1** (103.0 mg, 69.9 μmol) in degassed CH_2Cl_2 (20 mL) was treated with a saturated solution of $Zn(OAc)_2{\cdot}2H_2O$ in degassed MeOH (5 mL, excess), and the solution was stirred at room temperature for 1 h, during which its color changed from deep red to pink. UV/Vis analysis showed that by this time the reaction was complete. All volatiles were subsequently evaporated, and the remaining solid was stirred in a mixture of CH_2Cl_2 (20 mL) and degassed H_2O (20 mL) for 15 min. The organic layer was isolated, dried ($MgSO_4$), and filtered into a centrifuge vessel. Hexane (30 mL) was added to the filtrate, and the purple solution with a green tinge was concentrated to 10 mL and stored overnight at −30 °C. The resulting purple crystals of [5,10,15,20-tetrakis-(3,5-bis[(dimethylamino)methyl]-4-bromophenyl)porphyrinato]zinc(II) (**2**Zn) were isolated by centrifugation and dried in vacuo. Yield: 107.8 mg (99 %). UV/Vis (CH_2Cl_2): λ (log ε) = 427 (5.65), 562 (4.22), 603 nm (3.81); ^1H NMR: $\delta = 8.54$ (br s, 8H; β-H), 7.75 (br s, 8H; ArH), 3.15 (br s, 16H; CH_2N), 1.81 ppm (br s, 48H; $N(CH_3)_2$); $^{13}C\{^1H\}$ NMR: $\delta = 150.1$, 143.0, 134.4 (br), 131.7, 129.0, 120.5, 63.5 (br), 44.8 ppm (br); MS (ESI): *m*/*z* calcd for $C_{68}H_{81}Br_4N_{12}Zn$: 1451.4775 $[M+H]^+$; found: 1451.5000; elemental analysis: calcd (%) for $C_{68}H_{80}Br_4N_{12}Zn$: C 56.31, H 5.56, N 11.59, Zn 4.51; found: C 56.26, H 5.43, N 11.46, Zn 4.42. Crystals suitable for X-ray crystallography were grown by slow concentration of a saturated solution of **1**Zn in hexane.

2Zn: Synthesized according to the procedure used for the preparation of **1**Zn by using **2** (87.5 mg, 81.7 μmol) and a saturated methanolic solution of $Zn(OAc)_2{\cdot}2H_2O$ (5 mL, excess) to give [5,10,15,20-tetrakis(3,5-bis[(dimethylamino)methyl]phenyl)porphyrinato]zinc(II) (**2**Zn) as a purple solid. Yield: 92.6 mg (quantitative). UV/Vis (CH_2Cl_2): λ (log ε) = 427 (5.60), 562 (4.26), 603 nm (3.99); ^1H NMR: $\delta = 8.61$ (br s, 8H; β-H), 7.67 (br s, 8H; ArH), 7.20 (br s, 4H; ArH), 2.92 (br s, 16H; CH_2N), 1.74 ppm (br s, 48H; $N(CH_3)_2$); $^{13}C\{^1H\}$ NMR: $\delta = 150.1$, 143.0, 135.7 (br), 134.5 (br), 131.7, 129.0, 120.5, 63.7 (br), 44.9 ppm (br); MS (MALDI-TOF): *m*/*z* calcd for $C_{68}H_{85}N_{12}Zn$: 1134.89 $[M+H]^+$; found: 1134.72; elemental analysis: calcd (%) for $C_{68}H_{84}N_{12}Zn{\cdot}2H_2O$: C 69.75, H 7.58, N 14.35; found: C 69.46, H 6.98, N 14.08.

3Zn: Synthesized according to the procedure used for the preparation of **1**Zn by using **3** (79.9 mg, 62.3 μmol) and a saturated methanolic solution of $Zn(OAc)_2{\cdot}2H_2O$ (5 mL, excess) to give [5,10,15,20-tetrakis(3,5-bis-[methoxymethyl]-4-bromophenyl)porphyrinato]zinc(II) (**3**Zn) as red crystals. Yield: 81.9 mg (98 %). UV/Vis (CH_2Cl_2): λ (log ε) = 422 (5.76), 549 (4.28), 588 nm (3.25); ^1H NMR: $\delta = 8.81$ (s, 8H; β-H), 7.97 (s, 8H; ArH), 4.53 (s, 16H; CH_2O), 3.25 ppm (s, 24H; OCH_3); $^{13}C\{^1H\}$ NMR: $\delta = 150.1$, 142.1, 136.0, 133.6, 132.2, 122.5, 120.0, 74.2, 58.7 ppm; MS (MALDI-TOF): *m*/*z* calcd for $C_{60}H_{57}Br_4N_4O_8Zn$: 1346.008 $[M+H]^+$; found: 1346.013; elemental analysis: calcd (%) for $C_{60}H_{56}Br_4N_4O_8Zn$: C 53.53, H 4.19, N 4.16, Zn 4.86; found: C 53.42, H 4.16, N 4.08, Zn 5.08. Crystals suitable for X-ray crystallography were grown by slow diffusion of hexane into a concentrated solution of **3**Zn in CH_2Cl_2.

4Zn: Synthesized according to the procedure used for the preparation of **1**Zn by using **4** (90.7 mg, 93.8 μmol) and a saturated methanolic solution of $Zn(OAc)_2{\cdot}2H_2O$ (5 mL, excess) to give [5,10,15,20-tetrakis(3,5-bis-[methoxymethyl]phenyl)porphyrinato]zinc(II) (**4**Zn) as a red solid. Yield: 95.5 mg (quantitative). UV/Vis (CH_2Cl_2): λ (log ε) = 423 (5.77), 552 (4.26), 595 nm (3.25); ^1H NMR: $\delta = 8.81$ (s, 8H; β-H), 7.88 (s, 8H; ArH), 7.54 (s, 4H; ArH), 4.41 (s, 16H; CH_2O), 3.24 ppm (s, 24H; OCH_3); $^{13}C\{^1H\}$ NMR: $\delta = 150.2$, 143.3, 136.4, 133.2, 132.0, 126.1, 120.6, 74.5, 58.1 ppm; MS (MALDI-TOF): *m*/*z* calcd for $C_{60}H_{61}N_4O_8Zn$: 1028.37 $[M+H]^+$; found 1028.39; elemental analysis: calcd (%) for $C_{60}H_{60}N_4O_8Zn$: C 69.93, H 5.87, N 5.44, Zn 6.35; found: C 70.06, H 5.81, N 5.36, Zn 6.41.

DMBA–ZnTPP: DMBA (32 mg, 240 μmol) and hexanes (3 mL) were added to a solution of ZnTPP (20 mg, 30 μmol) in CH_2Cl_2 (3 mL). The resulting purple solution with a green tinge was allowed to evaporate slowly to about 2 mL at room temperature (2 days), during which purple crystals of DMBA–ZnTPP suitable for X-ray structure analysis formed. Yield: 20 mg (83 %). ^1H NMR: $\delta = 8.89$ (s, 8H; β-H), 8.15–8.12 (m, 8H; TPP ArH_{ortho}), 7.78–7.73 (m, 12H; TPP $ArH_{meta,para}$), 6.84 (t, $^3J_{H,H} = 6.6$ Hz, 1H; DMBA ArH_{para}), 6.75 (t, $^3J_{H,H} = 6.6$ Hz, 2H; DMBA ArH_{meta}), 5.81 (d, $^3J_{H,H} = 6.6$ Hz, 2H; DMBA ArH_{ortho}), −0.62 (s, 2H; CH_2N), −1.40 ppm (s, 6H; $N(CH_3)_2$); elemental analysis: calcd (%) for $C_{53}H_{41}N_5Zn$: C 78.27, H 5.08, N 8.61; found: C 78.15, H 5.03, N 8.68.

DMBABr–ZnTPP: Synthesized according to the procedure used for DMBA–ZnTPP by using ZnTPP (20 mg, 30 μmol) and DMBABr (45 mg, 240 μmol) to give DMBABr–ZnTPP as purple crystals. Yield: 25 mg (94 %). ^1H NMR: $\delta = 8.91$ (s, 8H; β-H), 8.24–8.21 (m, 8H; TPP ArH_{ortho}), 7.79–7.74 (m, 12H; TPP $ArH_{meta,para}$), 7.16 (d, $^3J_{H,H} = 6.6$ Hz, 1H; DMBABr ArH_3), 6.83–6.81 (m, 2H; DMBABr $ArH_{4,5}$), 6.25 (br, 1H; DMBABr ArH_6), 0.60 (br s, 2H; CH_2N), −0.36 ppm (br s, 6H; $N(CH_3)_2$);

elemental analysis: calcd (%) for $C_{53}H_{40}BrN_5Zn$: C 71.35, H 4.52, N 7.85; found: C 71.28, H 4.58, N 7.93.

NBrN–$(ZnTPP)_2$: Synthesized according to the procedure used for DMBA–ZnTPP by using ZnTPP (40 mg, 60 μmol) and NBrN (63 mg, 240 μmol) to give NBrN–$(ZnTPP)_2$ as purple crystals. Yield: 44 mg (94%). ^{1}H NMR: $\delta = 8.91$ (s, 16H; β-H), 8.25–8.22 (m, 16H; TPP ArH_{ortho}), 7.80–7.75 (m, 24H; TPP $ArH_{meta,para}$), 6.17 (t, $^3J_{H,H} = 6.6$ Hz, 1H; NBrN ArH_4), 5.54 (d, $^3J_{H,H} = 6.6$ Hz, 2H; NBrN $ArH_{3,5}$), −0.27 (br s, 4H; CH_2N), −1.18 ppm (br s, 12H; $N(CH_3)_2$); elemental analysis: calcd (%) for $C_{100}H_{75}BrN_{10}Zn_2$: C 73.80, H 4.65, N 8.61; found: C 73.51, H 4.78, N 8.74.

Determination of the ^{1}H NMR Spectroscopic Peak Positions of NBrN–ZnTPP at 213 K

A solution of ZnTPP (6.8 mg, 10 μmol) and NBrN (22 mg, 80 μmol) in $CDCl_3$ (500 μL) was cooled to 213 K in an NMR spectrometer. Analysis of the sample by ^{1}H NMR spectroscopy revealed a mixture of NBrN and NBrN–ZnTPP, whose peak positions are listed in Figure 11.

Determination of Binding Constants

Solutions containing ZnTPP (≈1 μM) and the appropriate amount (200–1000000 equiv) of Lewis base (DMBABr, DMBA, MBEBr, or MBE) in CH_2Cl_2 were prepared. The absorbance at the peak maximum of the resulting complex was monitored as a function of the concentration of Lewis base. In the plot of $(1/\Delta A)$ against (1/[Lewis base]), the intercept with the *x*-axis is −[binding constant].[75,94]

X-ray Crystal-Structure Determination

X-ray data were collected on a Nonius Kappa CCD diffractometer with rotating anode ($Mo_{K\alpha}$ radiation, $\lambda = 0.71073$ Å, graphite monochromator). SADABS[95] was used to correct for absorption. All structures were refined with SHELXL-97.[96] Hydrogen atoms were introduced at calculated positions and refined by riding on their carrier atoms. The analysis of the geometry, graphics, and structure validation were done with PLATON.[97] The structures of $[\mathbf{1}Zn]_\infty$, NBrN–$(ZnTPP)_2$, and DMBABr–ZnTPP were solved with SHELXS-86.[98] In $[\mathbf{1}Zn]_\infty$, one of the side chains is conformationally disordered and was refined with a disorder model. The structure also contains disordered solvent molecules in a solvent-accessible void of 180 Å^3, which was taken into account by back-Fourier transformation in the PLATON/SQUEEZE procedure.[97] The bridging bromophenyl group in NBrN–$(ZnTPP)_2$ is heavily disordered over the inversion center and was refined with isotropic displacement parameters. The structures of $[\mathbf{3}Zn]_\infty$, H_2O–ZnTPP, and DMBA–ZnTPP were solved with DIRDIF99.[99] The water molecule in H_2O–ZnTPP was refined with a disorder model. Further crystallographic details are given in Table 1. CCDC-625325–625330 contain the supplementary crystallographic data for $[\mathbf{1}Zn]_\infty$, $[\mathbf{3}Zn]_\infty$, NBrN–$(ZnTPP)_2$, DMBABr–ZnTPP, H_2O–ZnTPP, and DMBA–ZnTPP, respectively. These data can be obtained free of charge from The Cambridge Crystallographic Data Centre at http://www.ccdc.cam.ac.uk/data_request/cif.

Acknowledgements

The Dutch Council for Scientific Research (NWO) is gratefully acknowledged for financial support (D.M.T. and A.L.S) and for a Jonge Chemici scholarship (B.M.J.M.S. and R.J.M.K.G.).

[1] P. Jordan, P. Fromme, H. T. Witt, O. Klukas, W. Saenger, N. Krauß, *Nature* **2001**, *411*, 909–917.
[2] W. Kühlbrandt, D. N. Wang, Y. Fujiyoshi, *Nature* **1994**, *367*, 614–621.
[3] Z. Liu, H. Yan, K. Wang, T. Kuang, L. Gul, X. An, W. Chang, *Nature* **2004**, *428*, 287–292.
[4] G. McDermott, S. M. Prince, A. M. Freer, A. M. Hawthornthwaite-Lawless, M. Z. Papiz, R. J. Cogdell, N. W. Isaacs, *Nature* **1995**, *374*, 517–521.
[5] T. Pullerits, V. Sundström, *Acc. Chem. Res.* **1996**, *29*, 381–389.
[6] A. W. Roszak, T. D. Howard, J. Southall, A. T. Gardiner, C. J. Law, N. W. Isaacs, R. J. Cogdell, *Science* **2003**, *302*, 1969–1972.
[7] T. S. Balaban, *Acc. Chem. Res.* **2005**, *38*, 612–623.
[8] H. Tamiaki, *Coord. Chem. Rev.* **1996**, *148*, 183–197.
[9] M.-S. Choi, T. Yamazaki, I. Yamazaki, T. Aida, *Angew. Chem.* **2004**, *116*, 152–160; *Angew. Chem. Int. Ed.* **2004**, *43*, 150–158; .
[10] D. Holten, D. F. Bocian, J. S. Lindsey, *Acc. Chem. Res.* **2002**, *35*, 57–69.
[11] A. K. Burrell, D. L. Officer, P. Plieger, D. C. W. Reid, *Chem. Rev.* **2001**, *101*, 2751–2796.
[12] H. L. Anderson, *Chem. Commun.* **1999**, 2323–2330.
[13] H. Kurreck, M. Huber, *Angew. Chem.* **1995**, *107*, 929–947; *Angew. Chem. Int. Ed. Engl.* **1995**, *34*, 849–866.
[14] M. R. Wasielewski, *Chem. Rev.* **1992**, *92*, 435–461.
[15] C. M. Drain, J.-M. Lehn, *J. Chem. Soc. Chem. Commun.* **1994**, 2313–2315.
[16] R. V. Slone, J. T. Hupp, *Inorg. Chem.* **1997**, *36*, 5422–5423.
[17] E. Alessio, E. Ciani, E. Iengo, V. Y. Kukushkin, L. G. Marzilli, *Inorg. Chem.* **2000**, *39*, 1434–1443.
[18] E. Iengo, B. Milani, E. Zangrando, S. Geremia, E. Alessio, *Angew. Chem.* **2000**, *112*, 1138–1141; *Angew. Chem. Int. Ed.* **2000**, *39*, 1096–1099; .
[19] K. D. Benkstein, C. L. Stern, K. E. Splan, R. C. Johnson, K. A. Walters, F. W. M. Vanhelmont, J. T. Hupp, *Eur. J. Org. Chem.* **2002**, 2818–2822.
[20] E. Iengo, E. Zangrando, R. Minatel, E. Alessio, *J. Am. Chem. Soc.* **2002**, *124*, 1003–1013.
[21] K. E. Splan, M. H. Keefe, A. M. Massari, K. A. Walters, J. T. Hupp, *Inorg. Chem.* **2002**, *41*, 619–621.
[22] R. D. Hartnell, D. P. Arnold, *Organometallics* **2004**, *23*, 391–399.
[23] D. Sun, F. S. Tham, C. A. Reed, L. Chaker, P. D. W. Boyd, *J. Am. Chem. Soc.* **2002**, *124*, 6604–6612.
[24] S. J. Lee, J. T. Hupp, *Coord. Chem. Rev.* **2006**, *250*, 1710–1723.
[25] M. D. Ward, *Chem. Soc. Rev.* **1997**, *26*, 365–375.
[26] R. G. Ball, G. Domazetis, D. Dolphin, B. R. James, J. Trotter, *Inorg. Chem.* **1981**, *20*, 1556–1562.
[27] S. Mangani, E. F. Meyer, D. L. Cullen, M. Tsutsui, C. J. Carrano, *Inorg. Chem.* **1983**, *22*, 400–404.
[28] H. Segawa, N. Nakayama, T. Shimidzu, *J. Chem. Soc. Chem. Commun.* **1992**, 784–786.
[29] R. Krishna Kumar, S. Balasubramanian, I. Goldberg, *Chem. Commun.* **1998**, 1435–1436.
[30] M. L. Yates, A. M. Arif, J. L. Manson, B. A. Kalm, B. M. Burkhart, J. S. Miller, *Inorg. Chem.* **1998**, *37*, 840–841.
[31] E. J. Brandon, D. K. Rittenberg, A. M. Arif, J. S. Miller, *Inorg. Chem.* **1998**, *37*, 3376–3384.
[32] D. K. Rittenberg, K. Sugiura, A. M. Arif, Y. Sakata, C. D. Incarvito, A. L. Rheingold, J. S. Miller, *Chem. Eur. J.* **2000**, *6*, 1811–1819.
[33] S. Mikami, K. Sugiura, T. Maruta, Y. Maeda, M. Ohba, N. Usuki, H. Okawa, T. Akutagawa, S. Nisihara, T. Nakamura, K. Iwasaki, N. Miyazaki, S. Hino, E. Asato, J. S. Miller, Y. Sakata, *J. Chem. Soc. Dalton Trans.* **2001**, 448–455.
[34] A. M. Shachter, E. B. Fleischer, R. C. Haltiwanger, *J. Chem. Soc. Chem. Commun.* **1988**, 960–961.
[35] E. B. Fleischer, A. M. Shachter, *Inorg. Chem.* **1991**, *30*, 3763–3769.
[36] M. O. Senge, K. M. Smith, *J. Chem. Soc. Chem. Commun.* **1994**, 923–924.
[37] L. D. Sarson, K. Ueda, M. Takeuchi, S. Shinkai, *Chem. Commun.* **1996**, 619–620.
[38] A. K. Burrell, D. L. Officer, D. C. W. Reid, K. Y. Wild, *Angew. Chem.* **1998**, *110*, 122–125; *Angew. Chem. Int. Ed.* **1998**, *37*, 114–117; .
[39] F. Atefi, J. C. McMurtrie, P. Turner, M. Duriska, D. P. Arnold, *Inorg. Chem.* **2006**, *45*, 6479–6489.
[40] K. Ogawa, Y. Kobuke, *Angew. Chem.* **2000**, *112*, 4236–4239; *Angew. Chem. Int. Ed.* **2000**, *39*, 4070–4073.
[41] T. S. Kurtikyan, J. S. Ogden, R. K. Kazaryan, V. N. Madakyan, *Eur. J. Inorg. Chem.* **2003**, 1861–1865.

[42] B. Zimmer, M. Hutin, V. Bulach, M. W. Hosseini, A. De Cian, V. N. Kyritsakas, *New J. Chem.* **2002**, *26*, 1532–1535.
[43] U. Michelsen, C. A. Hunter, *Angew. Chem.* **2000**, *112*, 780–783; *Angew. Chem. Int. Ed.* **2000**, *39*, 764–767; .
[44] C. Ikeda, E. Fujiwara, A. Satake, Y. Kobuke, *Chem. Commun.* **2003**, 616–617.
[45] B. M. J. M. Suijkerbuijk, M. Lutz, A. L. Spek, G. van Koten, R. J. M. Klein Gebbink, *Org. Lett.* **2004**, *6*, 3023–3026.
[46] M. Albrecht, G. van Koten, *Angew. Chem.* **2001**, *113*, 3866–3898; *Angew. Chem. Int. Ed.* **2001**, *40*, 3750–3781; .
[47] B. M. J. M. Suijkerbuijk, D. M. Tooke, M. Lutz, A. L. Spek, G. van Koten, R. J. M. Klein Gebbink, unpublished results.
[48] E. Baciocchi, T. Del Giacco, A. Lapi, *Org. Lett.* **2004**, *6*, 4791–4794.
[49] J. A. Shelnutt, X.-Z. Song, J.-G. Ma, W. Jentzen, C. J. Medforth, *Chem. Soc. Rev.* **1998**, *27*, 31–41.
[50] This hexacoordination was unambiguously proven by the absence of disorder of the zinc atom in the direction perpendicular to the porphyrin plane, which rules out any dynamic shuttling of the zinc atoms between both sides of the porphyrin plane. This phenomenon was observed, for example, by Goldberg and co-workers.[78]
[51] M. P. Byrn, C. J. Curtis, Y. Hsiou, S. I. Khan, P. A. Sawin, S. K. Tendick, A. Terzis, C. E. Strouse, *J. Am. Chem. Soc.* **1993**, *115*, 9480–9497.
[52] P. Dastidar, H. Krupitsky, Z. Stein, I. Goldberg, *J. Inclusion Phenom. Mol. Recognit. Chem.* **1996**, *24*, 241.
[53] P. N. Taylor, A. P. Wylie, J. Huuskonen, H. L. Anderson, *Angew. Chem.* **1998**, *110*, 1033–1037; *Angew. Chem. Int. Ed.* **1998**, *37*, 986–989.
[54] A. D. Shukla, P. C. Dave, E. Suresh, A. Das, P. Dastidar, *J. Chem. Soc. Dalton Trans.* **2000**, 4459–4463.
[55] A. W. Kleij, M. Kuil, D. M. Tooke, A. L. Spek, J. N. H. Reek, *Inorg. Chem.* **2005**, *44*, 7696–7698.
[56] D. J. Ring, M. C. Aragoni, N. R. Champness, C. Wilson, *CrystEngComm* **2005**, *7*, 621–623.
[57] K. M. Barkigia, P. Battioni, V. Riou, D. Mansuy, J. Fajer, *Chem. Commun.* **2002**, 956–957.
[58] M. Vinodu, I. Goldberg, *New J. Chem.* **2004**, *28*, 1250–1254.
[59] Anderson surveyed the dihedral angles between porphyrins and *meso*-linked phenyl groups and found the mean angle to be 73° with a standard deviation of 9°: H. L. Anderson, *Chem. Commun.* **1999**, 2323–2330.
[60] M. Palacio, V. Mansuy-Mouries, G. Loire, K. Le Barch-Ozette, P. Leduc, K. M. Barkigia, J. Fajer, P. Battioni, D. Mansuy, *Chem. Commun.* **2000**, 1907–1908.
[61] E. Rose, M. Etheve-Quelquejeu, B. Andrioletti, *J. Porphyrins Phthalocyanines* **2003**, *7*, 375–381.
[62] R. K. Kumar, S. Balasubramanian, I. Goldberg, *Inorg. Chem.* **1998**, *37*, 541.
[63] N. Ehlinger, W. R. Scheidt, *Inorg. Chem.* **1999**, *38*, 1316–1321.
[64] C. K. Schauer, O. P. Anderson, S. S. Eaton, G. R. Eaton, *Inorg. Chem.* **1985**, *24*, 4082–4086.
[65] A. Zingg, B. Felber, V. Gramlich, L. Fu, J. P. Collman, F. Diederich, *Helv. Chim. Acta* **2002**, *85*, 333–351.
[66] S. M. LeCours, S. G. DiMagno, M. J. Therien, *J. Am. Chem. Soc.* **1996**, *118*, 11854–11864.
[67] S. G. DiMagno, V. S.-Y. Lin, M. J. Therien, *J. Am. Chem. Soc.* **1993**, *115*, 2513–2515.
[68] K. Kobayashi, M. Koyanagi, K. Endo, H. Masuda, Y. Aoyama, *Chem. Eur. J.* **1998**, *4*, 417–424.
[69] R. K. Kumar, A. Goldborth, I. Goldberg, *Z. Kristallogr. New Cryst. Struct.* **1997**, *212*, 383–384.
[70] X. Shi, S. R. Amin, L. S. Liebeskind, *J. Org. Chem.* **2000**, *65*, 1650–1664.
[71] P. Bhyrappa, S. R. Wilson, K. S. Suslick, *J. Am. Chem. Soc.* **1997**, *119*, 8492–8502.
[72] T.-L. Teo, M. Vetrichelvan, Y.-H. Lai, *Org. Lett.* **2003**, *5*, 4207–4210.
[73] A. J. Golder, D. C. Povey, J. Silver, Q. A. A. Jassim, *Acta Crystallogr. Sect. C* **1990**, *46*, 1210–1212.
[74] For these experiments, we focused on the Q-band region of the UV/Vis spectra, as the ratio between the two Q bands gives accurate information about the coordination environment around zinc. During the dilution experiment, the Soret band of each compound also underwent changes, but these were less informative.
[75] H.-J. Schneider, A. Yatsimirsky, *Principles and Methods in Supramolecular Chemistry*, John Wiley & Sons, New York, **1999**.
[76] T. Mizutani, K. Wada, S. Kitagawa, *J. Org. Chem.* **2000**, *65*, 6097–6106.
[77] D. Meyerstein, *Coord. Chem. Rev.* **1999**, *185–186*, 141–147.
[78] Y. Diskin-Posner, G. K. Patra, I. Goldberg, *J. Chem. Soc. Dalton Trans.* **2001**, 2775–2782.
[79] P. Bhyrappa, V. Krishnan, M. Nethaji, *J. Chem. Soc. Dalton Trans.* **1993**, 1901–1906.
[80] Calculated from the fact that at a concentration of 100 nM, 95% of **2**Zn is present in solution in the form of dimers, as deduced from the ratio of the Q bands.
[81] A. Satake, Y. Kobuke, *Tetrahedron* **2005**, *61*, 13–41.
[82] A. Mulder, T. Auletta, A. Sartori, S. Del Ciotto, A. Casnati, R. Ungaro, J. Huskens, D. N. Reinhoudt, *J. Am. Chem. Soc.* **2004**, *126*, 6627–6636.
[83] J. Deisenhofer, O. Epp, K. Miki, R. Huber, H. Michel, *Nature* **1985**, *318*, 618–624.
[84] M. Kunieda, H. Tamiaki, *J. Org. Chem.* **2005**, *70*, 820–828.
[85] S. I. Sasaki, H. Tamiaki, *J. Org. Chem.* **2006**, *71*, 2648–2654.
[86] M. Kunieda, H. Tamiaki, *Eur. J. Org. Chem.* **2006**, 2352–2361.
[87] Y. Saga, S. Akai, T. Miyatake, H. Tamiaki, *Bioconjugate Chem.* **2006**, *17*, 988–994.
[88] T. S. Balaban, A. D. Bhise, M. Fischer, M. Linke-Schaetzel, C. Roussel, N. Vanthuyne, *Angew. Chem.* **2003**, *115*, 2190–2194; *Angew. Chem. Int. Ed.* **2003**, *42*, 2140–2144; .
[89] T. S. Balaban, M. Linke-Schaetzel, A. D. Bhise, N. Vanthuyne, C. Roussel, *Eur. J. Org. Chem.* **2004**, 3919–3930.
[90] T. S. Balaban, M. Linke-Schaetzel, A. D. Bhise, N. Vanthuyne, C. Roussel, C. E. Anson, G. Buth, A. Eichhöfer, K. Foster, G. Garab, H. Gliemann, R. Goddard, T. Javorfi, A. K. Powell, H. Rösner, T. Schimmel, *Chem. Eur. J.* **2005**, *11*, 2267–2275.
[91] K. Sindelar, J. Holubek, E. Svatek, O. Matousova, J. Metysova, M. Protiva, *J. Heterocycl. Chem.* **1989**, *26*, 1325–1330.
[92] H. J. Reich, W. S. Goldenberg, A. W. Sanders, K. L. Jantzi, C. C. Tzschucke, *J. Am. Chem. Soc.* **2003**, *125*, 3509–3521.
[93] K. M. Smith, *Porphyrins and Metalloporphyrins*, Elsevier Scientific, Amsterdam, **1975**.
[94] H. A. Benesi, J. H. Hildebrand, *J. Am. Chem. Soc.* **1949**, *71*, 2703–2707.
[95] G. M. Sheldrick, SADABS, University of Göttingen, Göttingen (Germany), **1999**.
[96] G. M. Sheldrick, SHELXL-97, Program for Crystal-Structure Refinement, University of Göttingen, Göttingen (Germany), **1997**.
[97] A. L. Spek, *J. Appl. Crystallogr.* **2003**, *36*, 7–13.
[98] G. M. Sheldrick, SHELXS-86, University of Göttingen, Göttingen (Germany), **1986**.
[99] P. T. Beurskens, G. Admiraal, G. Beurskens, W. P. Bosman, S. Garcia-Granda, R. O. Gould, J. M. M. Smits, C. Smykalla, The DIRDIF99 Program System, Technical Report of the Crystallographic Laboratory, University of Nijmegen, Nijmegen (The Netherlands), **1999**.

Received: March 9, 2007
Published online: June 1, 2007

